Title

Dynamic P-glycoprotein expression in early and late memory states of human CD8 + T cells and the protective role of ruxolitinib

Authors

Biwott, Kipchumba
Singh, Parvind
Baráth, Sándor
et al.

Publication Date

2025

DOI

10.1016/j.biopha.2024.117780

Biomedicine & Pharmacotherapy 182 (2025) 117780

Contents lists available at ScienceDirect

Biomedicine & Pharmacotherapy

journal homepage: www.elsevier.com/locate/biopha

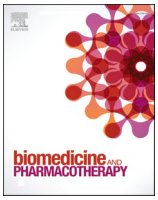

Dynamic P-glycoprotein expression in early and late memory states of human CD8 + T cells and the protective role of ruxolitinib

Kipchumba Biwott [a,b,d], Parvind Singh [c], Sándor Baráth [c], James Nyabuga Nyariki [d], Zsuzsanna Hevessy [c], Zsolt Bacso [a,b,e,*]

[a] Department of Biophysics and Cell Biology, Faculty of Medicine, University of Debrecen, Debrecen 4032, Hungary
[b] Doctoral School of Molecular Cell and Immune Biology, University of Debrecen, Debrecen 4032, Hungary
[c] Department of Laboratory Medicine, Faculty of Medicine, University of Debrecen, Debrecen 4032, Hungary
[d] Department of Biochemistry and Biotechnology, Technical University of Kenya, Kenya
[e] Dean's office, Faculty of Pharmacy, University of Debrecen, Debrecen 4032, Hungary

ARTICLE INFO

Keywords:
P-glycoprotein
Cytotoxic T lymphocyte
CTL memory subsets
Ruxolitinib
JY cells
TCR activation

ABSTRACT

ABCB1/MDR-1/P-glycoprotein (Pgp) is an ABC transporter responsible for cancer cell multi-drug resistance. It is expressed in cytotoxic T lymphocytes (CTL). Eliminating sensitive cancer cells during high-dose chemotherapy can also damage immune cells. Our study aimed to assess which maturing human CD8 + CTL memory subsets may be affected based on their Pgp protein expression. In an *in vitro* CTL differentiation model system, we tracked the maturation of naive, effector, and memory cells and the expression of Pgp. This system involves co-culturing blood lymphocytes with proliferation-inhibited JY antigen-presenting B-lymphoblastoid cells expressing HLA-I A2. These JY-primed maturing CTLs were TCR-activated using beads, and the effect of the maturation-modifying JAK1/2 inhibitor ruxolitinib was examined. Multidimensional analysis identified six major CTL subsets: naive, young memory (Tym), stem cell memory (Tscm), central memory (Tcm), effector memory (Tem), and effectors (Te). These subsets were further divided into thirteen specific subsets: TymCD127 +, TymCD127-, Tscm, TcmCD95 +, TcmCD73 +CD95 +, TcmCD95+CD127 +, TcmPD1 +, TemCD95 +, TemraCD127 +, TemraCD127-, TeCD95 +, and TeCD73 +CD95 +. Pgp expression was detectable in naïve cells and dynamically changed across the thirteen identified subsets. Increased Pgp was detected in young memory T cells and in Tscm, TcmCD95 +, and TcmPD1 + human CTL subsets. Unlike other transiently appearing memory cells, the number of cells in these core Pgp-expressing memory subsets stabilized by the end of the contraction phase. Ruxolitinib treatment downregulated effector T-cell polarization while upregulating small memory subsets expressing Pgp. In conclusion, activation increased Pgp expression, whereas ruxolitinib treatment preserved small early and late memory subset core that primarily expressed Pgp.

1. Introduction

ABCB1/MDR-1/P-glycoprotein (Pgp), an ATP-binding cassette (ABC) transporter, plays a pivotal role in chemoresistance by expelling xenobiotic substances from cells and protecting tissues against toxins. It is highly expressed in critical barriers, such as the blood-brain barrier and the placenta, safeguarding sensitive tissues from harmful compounds [1,2]. Beyond its canonical function in multidrug resistance (MDR) tumors [3], Pgp contributes to the body's chemo-immunity defense system [1]. It also exhibits non-canonical roles, such as releasing endogenous molecules in specific cell types, including adrenal aldosterone export [4]. Pgp expression can be induced under oxidative stress or inflammatory conditions and is found in most immune cells [5]. These include innate and adaptive immune cells like monocytes, natural killer cells, dendritic cells, mucosal-associated invariant T-cells (MAIT), B cells, and T lymphocytes. While high Pgp expression in immune cells has been linked to poor outcomes in autoimmune disease treatments, it can also confer beneficial effects. For example, during chemotherapy, the immune system's antiviral responses often persist [6,7], potentially due to Pgp expression in long-lived antiviral T cells. This enables immune

* Corresponding author at: Department of Biophysics and Cell Biology, Faculty of Medicine, University of Debrecen, Debrecen 4032, Hungary.
E-mail addresses: kipchumba.biwott@med.unideb.hu (K. Biwott), parvind.singh@med.unideb.hu (P. Singh), barath.sandor@med.unideb.hu (S. Baráth), nyabukaj@tukenya.ac.ke (J.N. Nyariki), hevessy@med.unideb.hu (Z. Hevessy), bacso@med.unideb.hu (Z. Bacso).

https://doi.org/10.1016/j.biopha.2024.117780
Received 27 September 2024; Received in revised form 14 December 2024; Accepted 20 December 2024
Available online 30 December 2024

cells to withstand the harsh tumor microenvironment and influences the bioavailability of immune-modulating corticosteroids [8–10].

In tumors, elevated Pgp levels in cancer cells drive chemoresistance, complicating treatment [11]. High-dose chemotherapy can effectively target tumor cells but may also damage non-target immune cells, including tumor-infiltrating lymphocytes, leading to lymphocytopenia and an increased risk of severe infections [11]. Despite this, Pgp-expressing memory T cells, which are highly resilient, often survive chemotherapy. These cells play a critical role in immune recovery, exhibiting stress resistance, proliferation, differentiation potential, and longevity [7,12]. Among them, CD8 + memory T cells are especially significant for immune defense, with young Pgp-expressing memory T cells (Tym) showing particular promise in tumor-targeted therapies due to their unique functional properties [13].

Ruxolitinib (RUX), an FDA-approved inhibitor targeting JAK1/2, has garnered attention in the treatment of various blood cancers, including myeloproliferative neoplasms/myelodysplastic syndrome, polycythemia vera, acute and chronic lymphoblastic leukemia, and myelofibrosis (MF) [14,15]. Its expanding applications are supported by effectiveness demonstrated in recent successful treatment studies, including protocol development for managing the hyperinflammatory state of COVID-19 and reducing PD-1 expression in MF, where PD-1 is overexpressed as T cells undergo persistent activation [14,16,17].

Studies suggest that ruxolitinib affects T-cell maturation. It shifts T cell subsets towards CD8 + phenotypes, particularly by increasing naive (Tn) and central memory T cells (Tcm) while decreasing effector memory (Tem) and effector T cells (Te), a crucial aspect of its efficacy in managing MF [15].

The study of CD8 + memory cells is a dynamic area of research due to their crucial role in the persistence of immune responses, particularly in preventive vaccinations and cancer immunology. In organ transplantation, CD8 + memory stem cells are key in determining transplant success. Memory stem cells were first described in commonly used murine models investigating graft versus host disease (GVHD) [15]. Gattinoni [18] identified this highly proliferative T-cell subset in humans expressing CD95 and CD122. The subset can easily be mistaken for MAIT cells, which also exhibit high Pgp expression [7,19]. Notably, young memory T cells (Tym), as described by Murata [13], display drug resistance and differentiate into Tcm cells, which express CD73 and demonstrate both drug resistance and aldehyde dehydrogenase 1 (ALDH1) activity. Over the past two decades, CD8 + populations expressing the IL-7 receptor (CD127) with efflux activity have been recognized [20]. However, our understanding of Pgp expression across CD8 + T-cell phenotypes remains incomplete, and the potential functional role of Pgp in memory T-cell maturation is still unclear.

We investigated maturation changes in CD8 + T-cell subsets using a human in vitro CTL differentiation model. This model generates long-lived memory T-cell subsets over a one-month culture period, following the priming of T cells derived from peripheral blood mononuclear cells (PBMCs) with JY antigen-presenting cells (APCs) [21]. These JY APCs, derived from B lymphoblastoid leukemia cells, express high levels of HLA-I A2 and HLA-II DQ and primarily initiate MHC class-I-restricted changes [22].

T-cell activation and maturation require three critical signals: antigen-specific recognition, co-stimulatory signals, and interleukin-mediated signaling. Receptor-ligand interactions between tumor-antigen-presenting APCs and T cells play a pivotal role in neoplastic hematological disorders. Prior research has demonstrated that JY cells can induce tumor-specific cytotoxic T-lymphocytes (CTLs), offering a potential approach for myeloma immunotherapy [22–25]. The JY cell line-induced, MHC-I-restricted cellular immune response efficiently generates allogeneic, anti-tumor, or virus-specific CD8 + CTLs from PBMCs [21–24]. While standard in vitro T-cell activation methods, such as CD3/CD28 bead-based approaches, have been succeeded by advanced techniques like lipid vesicle-based activation [26], the JY cell-induced system is likely more efficient due to its physiological mimicry of natural cell-cell interactions.

To assess the progression of subset changes, we compared the initial PBMC composition, serving as a baseline snapshot, with the maturation profile after one month of JY exposure. Additionally, a shorter, 3-day CD3/CD28 activation was employed to capture two intermediate snapshots, offering deeper insight into subset dynamics. By incorporating ruxolitinib treatment, known to influence T-cell maturation, we further delineated phases of differentiation, enhancing our understanding of memory subset dynamics. Throughout this process, we monitored P-glycoprotein (Pgp) expression across maturing T-cell subsets.

This study identified distinct long-lived CD8 + T-cell subsets expressing Pgp, which were preserved through progressive memory cell maturation. Our system successfully replicated the adaptive immune response's natural tendencies, with effector properties upregulated and naive and intermediate memory T cells downregulated during both short-term CD3/CD28 activation and long-term JY cell stimulation. Furthermore, ruxolitinib exposure delayed effector differentiation and increased the population of CD127-expressing cells. These findings suggest that elevated Pgp expression is critical for maintaining long-lived memory cells in human cytotoxic T lymphocytes.

2. Materials and Methods

2.1. Antibodies and chemicals

The following fluorescently-labeled monoclonal antibodies (mAbs) were applied. Mouse anti-human CD16 Fluorescein isothiocyanate (FITC), CD19 Phycoerythrin (PE), CD56 Peridinin Chlorophyll Protein-Cyanine 7 (PC7), and CD62L Pacific Blue (Beckman Coulter,Brea, CA, USA). Mouse anti-human CD3 Peridinin Chlorophyll Protein-Cyanine 5.5 (PerCP-Cy5.5), CD4 Pacific Blue, CD45 RA FITC, and CD8 Allophycocyanin-Hilite7 (APC-H7) (Becton Dickinson, Franklin Lakes, NJ, USA). Mouse anti-human CD45 Pacific Orange (PO) (EXBIO Prague, Czech Republic). Mouse anti-human CD73 PE (Sony Biotechnology Inc., San Jose, CA, USA). Mouse anti-human CD95 PE-Cyanine7 and CD127 PE-Cyanine5.5 (Thermo Fisher Scientific, Waltham, MA, USA). Mouse anti-human CD279 (PD-1) Allophycocyanin-Cyanine7 (APC-Cy7) (BioLegend, San Diego, CA, USA). The anti-human CD8 (OKT8) PO and Pgp (15D3) Alexa Fluor 647 dye-labeled mouse mAbs were produced in-house from hybridoma and mouse ascites.

The anti-human CD8 mouse mAb was isolated from the supernatant of OKT8 hybridoma cells. OKT8 cells were cultured in RPMI medium, and the supernatant was collected and purified using a Protein-A column at 4°C.

The 15D3 anti-human Pgp mouse mAb was purified from mouse ascites [27]. One million 15D3-hybridoma cells were injected intraperitoneally into female BALB/C and Swiss nude mice aged ten weeks. Mice were housed in the animal house of the University of Debrecen, Life Science Building, Hungary, where conditions were controlled to maintain a temperature range of 21–25°C and a 12-hour light/dark cycle. The mice had free access to standard mice pellets and water ad libitum within standard mice cages. On the 14th day of post-injection, ascites were collected aseptically from the mice and stored at −80°C. The collected ascites were purified using a protein-G column kit (Thermo Fisher Scientific NAb™ Protein G Spin Kit), following the manufacturer's instructions [27].

The isolated 15D3 and OKT8 mAbs protein concentration was measured with a NanoDropTM OneC microvolume UV-Vis Spectrophotometer at 280 nm. 0.02 % sodium azide solution was added to the purified antibodies, which were then stored at four °C or for a long time at −20°C. Furthermore, according to manufacturer instructions, Alexa Fluor and PO-labeled mAbs were prepared for direct immune-labeling purposes (Thermo Fisher Scientific, Waltham, MA, USA).

The chemicals not specifically indicated were purchased from Thermo Fisher Scientific (Waltham, MA, USA), or Sigma-Aldrich (St.

Louis, MO, USA).

2.2. Cell lines and generation of cytotoxic T lymphocytes

The JY cell line is a human Epstein–Barr virus-transformed B-lymphoblastoid cell line expressing a high density of MHC class I A2 and class II DR on the surface plasma membrane [21]. Cell lines were maintained in RPMI 1640 medium (Sigma- Aldrich, (St. Louis, MO, USA) supplemented with sodium bicarbonate, glucose, pyruvate, MEM non-essential amino acids, GlutaMAX, gentamycin, or ampicillin, and 10 % heat-inactivated FCS (SEBAC, Aidenbach, Germany) (complete medium) in a 5 % CO_2 at 37°C.

CTLs were generated from human peripheral blood lymphocytes (PBL). First, peripheral blood mononuclear cells (PBMCs) were isolated from leukocyte-enriched buffy coats from healthy blood. PBMCs were separated by a standard density gradient centrifugation with Ficoll-Paque Plus (Amersham Biosciences, Uppsala, Sweden). Then, monocytes were removed from PBMCs by positive selection using immunomagnetic cell separation with anti-CD14-conjugated microbeads (Miltenyi Biotec, Bergisch Gladbach, Germany), according to the manufacturer's instruction. The resultant PBLs were cultured at a density of 2–5 million cells/ml for a couple of days in T75 tissue culture flasks in a complete RPMI medium supplemented with 10 mM Hepes buffer (pH 7.3) and 50 μM 2-mercaptoethanol (SERVA, Heidelberg, Germany), until it was used for experiments or cells were frozen for more extended storage. When required, 20 IU of human recombinant IL-2 (PeproTech, Cranbury, NJ, USA) was also included in the complete medium.

CTLs were generated by priming PBLs with heat-treated JY antigen-presenting cells in mixed cultures of 4:1 ratio according to procedures outlined in previous research. [21]. The JY cells were heat shocked at 45°C for 2 hours to block their proliferation. After the third day of cell mixing, 20 IU of IL-2 was added to the culture medium every third day, and the cells were cultured for 14 days [21]. Then, the APC priming was repeated for another 14-day cycle. It is known that long-term low-level IL-2 promotes memory T-cell development [28].

2.3. Experimental setup to measure the change in phenotypes and Pgp expression

The phenotypes of peripheral blood lymphocytes and Pgp expression were measured in PBLs that were unprimed (JY-non-exposed) and after JY-exposure (JY-primed). Multicolor flow cytometric measurements were carried out to determine the change in the population proportion and Pgp expression in different populations (T, B, NK, and NKT, CD4 +, and CD8 + T cells). Four independent repeated experiments were carried out (Table 1A).

2.4. Experimental setup of the T cell activation and treatment

CTL maturation experiments used the JY-primed PBLs (JY-exposed cells) after the one-month subset differentiation period. The unprimed (JY-non-exposed) control lymphocytes compared in the activation experiments were from the same two donor sources as the JY-exposed CTLs. The unprimed experiments were repeated 3 times, giving 12 FCS (flow cytometry standard) files in the 4 groups. The JY-primed experiments were repeated 4 times giving 16 FCS files in the 4 activation/treatment groups. That gave altogether 28 files. The experimental setup is shown in Table 1B.

TCR-activation of cells was achieved by coating wells of a 24-well plate with 2 μg/ml antibody of the CD3/CD28 Dynabeads and incubating overnight at 4°C. Then, excess Ab was removed with PBS wash and one million cells from JY-exposed primed and JY-non-exposed unprimed cells were added separately to individual wells (TCR-activated cells). Ruxolitinib (Incyte Corp., Wilmington, DE), was added to wells separately containing CD3/28 (activated and RUX treated cells). RUX was added to the wells that contained only the cells (RUX-only treated cells), and untreated/unstimulated cells, (control cells) were used. The activations and treatments were done for 72 hours.

Table 1
Experimental design. The experiment was designed to test T-cell activation and treatment. (A) Peripheral blood lymphocytes (PBLs) were unprimed (JY-non-exposed), and after JY-exposure (JY-primed) for 28 days. Then cells were used to assess the change in population proportion and Pgp expression. (B) PBLs were unprimed (JY-non-exposed), and after JY-exposure (JY-primed) for 28 days. On these cells activation and treatment was performed where they were either activated with CD3/28 beads, or treated with Ruxolitinib, or activated and treated together (CD3/28 +Ruxolitinib) and control (unstimulated and untreated). CD8 + CTLs were measured using flow cytometry, and multidirectional data were analyzed to classify the CTL subsets.

A			
PBLs	**Time of exposure**		
Non-exposed to JY-cells, unprimed PBLs (prior in vivo T cell maturation)	-	**Flow cytometry measurements after the JY-priming were performed and data were analyzed with sequential gating**	
JY-priming (PBLs exposed to JY-cells (in vitro CTL maturation)	28 days of JY-cell exposure (2 times of 14-day cycles)		
B			
PBLs	**Time of exposure**	**Activation/ treatment (72 hours)**	
Non-exposed to JY-cells, unprimed PBLs (prior in vivo T cell maturation)	-	**Unstimulated/ untreated (control)** **Treated (ruxolitinib)** **Activated (CD3/ 28)** **Activated (CD3/ 28) and treated (ruxolitinib)**	**Flow cytometry measurements after the activation/ treatment and multidimensional data analysis was performed**
JY-priming (PBLs exposed to JY-cells (in vitro CTL maturation)	28 days of JY-cell exposure (2 times of 14-day cycles)	**Unstimulated/ untreated (control)** **Treated (ruxolitinib)** **Activated (CD3/ 28)** **Activated (CD3/ 28) and treated (ruxolitinib)**	

2.5. Flow cytometry

Cellular surface staining of lymphocytes was performed using mAbs detailed above. Briefly, cells were incubated with mAbs for 15 minutes at room temperature, followed by washing with PBS at 1600 RPM for 5 minutes. Later, cells were suspended in 400 μL of PBS for acquisition. Samples were measured in eight fluorescence channels with FACS Canto II, using BD FACSDiva v6.1.3 (BD Bioscience, Franklin Lakes, NJ, USA). 100,000 events per sample were collected, and the data were analyzed using FlowJo v10.9.0 (TreeStar Inc., Ashland, OR, USA).

The data were preprocessed (cleaned, gated, down-sampled, and concatenated) before machine learning algorithms. Briefly, PeacoQC for quality control was used [29] followed by the removal of doublets based on forward scatter (FSC) area vs height and FSC area vs width parameters. White blood cells (WBCs) were gated based on light scattering parameters (FSC vs SSC). This was followed by CD45 + lymphocytes that were gated on CD45 vs SSC. Subsequently, lymphocyte subsets were gated based on different markers shown in Suppl. Fig. 1.

For Pgp-expressing lymphocyte phenotyping, sequential gating was applied, as shown in Supplementary figure 1. For CTL phenotypes, multidimensional analysis was performed using the FlowJo plugin.

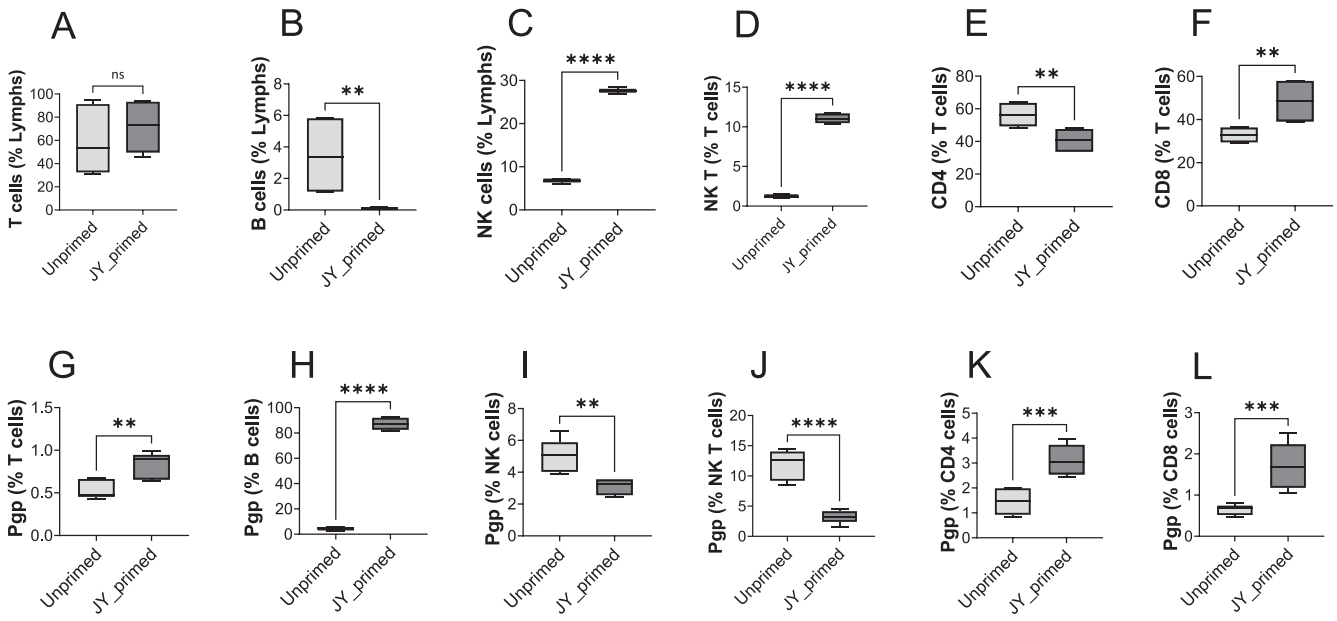

Fig. 1. Phenotypes of the peripheral blood lymphocytes identified and Pgp-expression in the unprimed and JY-primed cultures. Flow cytometric analysis was employed to determine the rise of the population proportion of T, B, NK cells, and NK T cells and CD4 + and CD8 + T subsets in both cultures of the JY-primed and unprimed cells. Changes in the levels of different immune cells and the percentage of Pgp-positive cells were calculated and analyzed, averaging the results of the measurements using a student *t*-test. (Statistical significance key: ns non-significant, **$p < 0.01$, ***$p < 0.001$, ****$p < 0.0001$, $n = 4$).

Sequential gating was performed to clean and gate CD8 + T cells before multidimensional analysis (Suppl. Fig. S2 for visualization). 3200 CD8 + cells were down-sampled from each of the 28 files resulting in N = 89,600 selected CD8 + human T lymphocytes. The data were concatenated in a single file used for multidimensional analysis.

Dimensionality reduction was performed using Uniform Manifold Approximation and Projection (UMAP) to visualize the high-dimensional data [30]. FlowSOM was utilized to construct self-organizing maps and identify meta-clusters of T cells [31], and the number of clusters was optimized through multiple clustering iterations with different numbers of meta-clusters to prevent over- and under-clustering (Suppl. Fig. S3). Slight over-clustering was preferred to avoid missing out on less expressive clusters. The immune clusters identified by FlowSOM were overlaid onto individual samples, and the percentage of these clusters among CD8 lymphocyte cells was exported for statistical comparison across different experimental conditions.

2.6. Statistical analysis

Kolmogorov–Smirnov and Shapiro–Wilk normality tests were used to test the normality of data distribution. For non-normal distributed, nonparametric variables, the Mann-Whitney test, and the normally distributed parametric variables, Student's *t*-test was used to calculate the significant differences. One-way ANOVA with Tukey's post hoc test for multiple comparisons was employed for internal comparison with the significance level set at $p < 0.05$. Statistical analysis was performed using GraphPad Prism v9.0 (GraphPad Software, Inc., San Diego, USA). A chi-square test of independence was conducted in Excel to determine whether the measured magnitudes of CTL subsets varied significantly across different activations and treatments. Post hoc comparisons were adjusted using the Bonferroni correction to account for multiple tests. The effect size was calculated using Cramer's V and interpreted as large, medium, small, or negligible based on established thresholds.

2.7. Ethics approval

Blood samples were obtained with the written consent of voluntary healthy donors through individual donations at the Regional Blood Center of the Hungarian National Blood Transfusion Service (Debrecen, Hungary). This collection was conducted under the written approval (OVSzK 3572–2/2015/5200) of the Director of the National Blood Transfusion Service and the Regional and Institutional Ethics Committee of the University of Debrecen, Faculty of Medicine (Hungary).

3. Results

3.1. JY-priming predominantly generates specific CD8 + T cell phenotypes and increases P-glycoprotein expression in these populations

Human peripheral blood lymphocytes were cultured with proliferation-inhibited JY cells. The JY cell line, derived from B-lymphoblasts, expresses high levels of MHC class I A* 02:01 proteins on its surface, functioning as a potent antigen-presenting cell. This induces a strong CD8 + cellular allotype immune response in mixed lymphocyte cultures. In previous studies, we demonstrated the cytotoxic efficiency of the generated CTL clones, showing their specific and compelling activity against JY target cells [21]. The measurements in this study were primarily conducted using 8-color flow cytometry on live cells.

While the overall frequency of T cells did not significantly increase in JY-primed lymphocytes compared to unprimed/non-exposed cells (Fig. 1A), CD8 + T cells were significantly upregulated (Fig. 1F). Notably, CD4 + T cells were significantly decreased (Fig. 1E), underscoring the efficiency of MHC I restriction. Additionally, the frequency of NK and NK T cells significantly increased (Fig. 1C-D). In contrast, the proportion of B cells decreased dramatically in JY-primed cells compared to JY-non-exposed cells (Fig. 1B).

We also monitored the proportion of Pgp-expressing cells across various T-cell phenotypes in PBMC-derived lymphocyte cultures. Overall, the percentage of Pgp-positive cells increased significantly within the T-cell population (Fig. 1G). Specifically, the Pgp-expressing fraction increased in both CD4 + and CD8 + T cells (Fig. 1K and L), while it decreased considerably in NK and NK T cells (Fig. 1I and J). The significant increase in Pgp-expressing B cells is not important due to the substantial decrease in the overall number of B cells (Fig. 1B and H).

3.2. Memory subpopulations identified during JY-primed CD8 + T cell maturation

The most common T-cell characterization uses the CD45RA (or RO) marker to distinguish naive from memory cells and CD62L (or CCR7) to further differentiate naive and central memory from peripheral effectors and Temra cells (terminal effector memory T cells or T effector memory cells re-expressing RA antigen).

According to this conventional characterization, naive T cells are CD45RA+CD62L+ , central memory cells (Tcm) are CD45RA-CD62L+ , effector cells (Te) are CD45RA-CD62L-, and terminally differentiated effector cells (Temra) are CD45RA+CD62L- [13]. Additional subsets within these categories were identified based on existing literature [32–35] (markers in Fig. 2i).

We used multi-parametric flow cytometry on PBLs and JY-primed cultures, applying specific cell surface markers for labeling (Fig. 2i). Immune clusters were assigned based on marker expression levels, as shown in the heat map (Fig. 2i), and the data were consolidated into a single dataset. FlowSOM identified immune clusters, which were overlaid onto individual samples, and their percentages among CD8 + lymphocytes were compared. UMAP was used for dimensionality reduction to visualize high-dimensional data (Fig. 2ii). In both JY-exposed and non-exposed CTLs, we identified 13 distinct CD8 + subsets: naive T cells, TeCD73 +CD95 + , TeCD95 + , TemraCD127 + , TemraCD127-, TymCD127 + , TymCD127-, Tscm, TemCD95 + , TcmCD95+CD127 + , TcmCD73 +CD95 + , TcmCD95 + , and TcmPD1 + .

3.3. P-glycoprotein-expressing CTL subsets were identified in both JY-primed and unprimed cultures

Among the 13 identified subsets, five exhibited significantly elevated levels of the multi-drug resistance protein Pgp: TymCD127 + , TymCD127-, Tscm, TcmCD95 + , and TcmPD1 + (Fig. 2i). Notably, the highest Pgp levels were observed in the PD1-expressing central memory Tcm (TcmPD1 +) subset, which is a novel finding. This was followed by the young memory CD127 + subset (TymCD127 +) as described by Murata [13]. The remaining three subsets—TymCD127-, Tscm, and TcmCD95 + —showed progressively lower levels of Pgp.

We also assessed the average Pgp expression in these memory subpopulations under various maturation, activation, and treatment conditions (Suppl. Fig. S4). Analysis indicated that the TymCD127 + and TcmPD1 + memory subpopulations exhibited the highest Pgp expression. Furthermore, priming, activation, and ruxolitinib treatment all

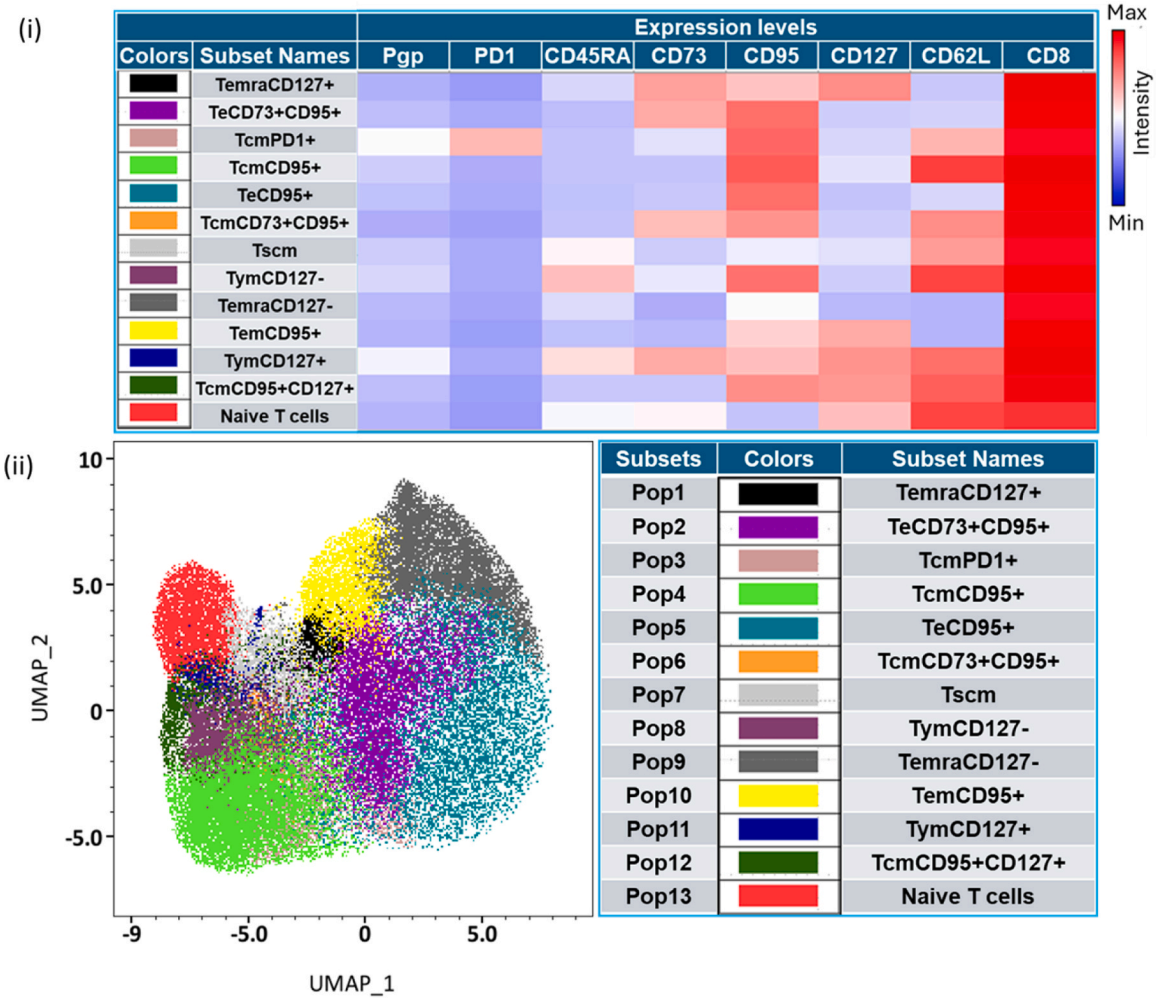

Fig. 2. Immune clusters identified with the heat map showing T cell phenotypes. Heat map showing the expression of different markers and Pgp for each phenotype (i); Dimensionality reduction (UMAP) and clustering (FlowSOM) of flow cytometric data are presented. The X-axis represents UMAP_1, the Y-axis represents UMAP_2, and the legend of clusters, which showed significant differences among treatments, are shown. CD8 + clusters identified as naive T cells, TeCD73 +CD95 + , TeCD95 + , TemraCD127 + , TemraCD127-, TymCD127 + , TymCD127-, Tscm, TemCD95 + , TcmCD95+CD127 + , TcmCD73 +CD95 + , TcmCD95 + , and TcmPD1 + (ii). It was named based on surface markers expressed according to the heat map. Conventional naive T cells are CD45RA+CD62L+ , those of central memory T cells are CD45RA-CDL62 + , the effectors are CD45RA-CD62L-, and those of TemraCD127- are CD45RA+CD62L-.

maintained significant levels of Pgp, with RUX showing a tendency to further increase Pgp expression.

It is important to note that high levels of Pgp are not necessarily required for its physiological function. Even quiescent naive T cells displayed measurable levels of cell surface Pgp. The elevated Pgp expression observed in cancer cells is a specific adaptation that facilitates multi-drug resistance (MDR) to chemotherapy.

3.4. Phenotypic polarization reflects typical adaptive immune responses in the JY-primed CTL maturation model following TCR activation

Our objective was to differentiate T-cell effector and memory phenotypes by exposing PBLs to antigen-presenting B cells (JY cell line-induced -priming) during the culture period. We measured CD8 + T cell polarization under various activation conditions, resulting in a comprehensive dataset comprising 89,600 CD8 + cells (see Methods). We constructed a contingency table to assign each cytotoxic T lymphocyte (CTL) phenotypic subset to specific cells across different activation and treatment conditions (Suppl. Table S1). Supplementary figure 5 and Figs. 3–5 illustrate the observed changes in all subsets across treatment and maturation stages. In this extensive dataset, nearly all CD8 + T cell activation changes were statistically significant, with non-significant changes marked as 'ns' in Supplementary figure 5 and Figs. 3–5. We also calculated the effect sizes of these changes (details provided in the Methods), highlighting the biological relevance of these statistically significant variations. Subsets with large effect sizes, which predict significant immunological alterations, are emphasized with bold names in Supplementary figure 5 and Figs. 3–5.

3.4.1. Differentiation of CD8 + T cell subsets derived from human peripheral blood lymphocytes in response to TCR activation

Fig. 3 (and Suppl. Fig. S5A) illustrates the initial antigen encounter and the expansion phase of the adaptive T cell immune response following seventy-two hours of TCR activation in unprimed PBLs (JY-non-exposed cells). In the upper panel of Fig. 3i, color-coded subpopulations shift into different colors, visually confirming cell maturation changes as shown in the UMAP cluster map.

Theoretically, subsets initially present in the PBL sample will change

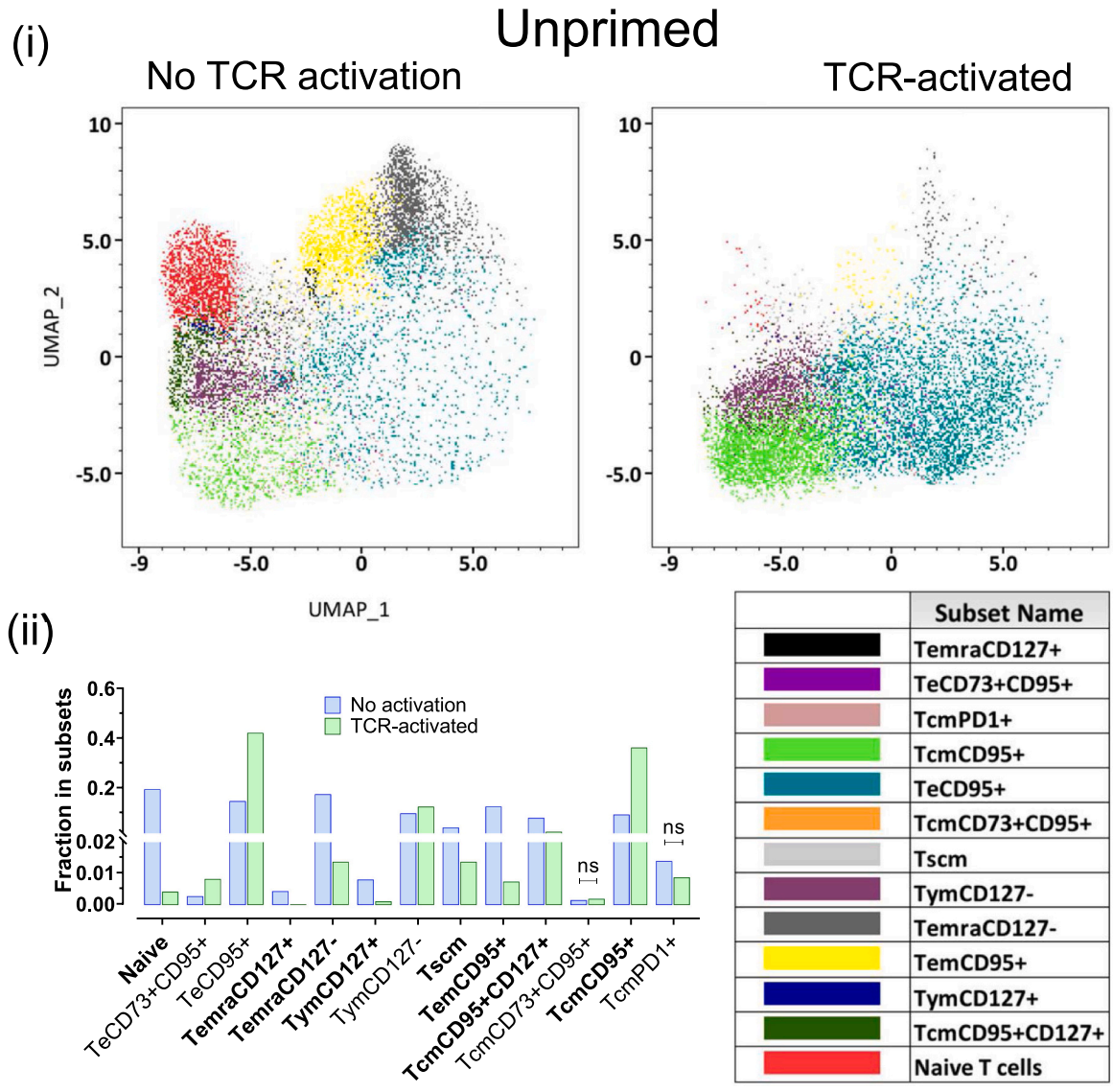

Fig. 3. Changes in CD8 + T cell subset sizes from human peripheral blood lymphocytes in response to TCR activation after seventy-two hours (JY-non-exposed cells). (i) The upper panel presents a UMAP cluster map with color-coded subpopulations, visually confirming maturation changes. (ii) The lower panel displays a bar chart showing changes in the same data set. All changes are statistically significant except those marked "ns" (non-significant). Subsets in bold indicate a large effect size, suggesting significant immunological effects. Non-bolded subsets represent medium or small effect sizes.

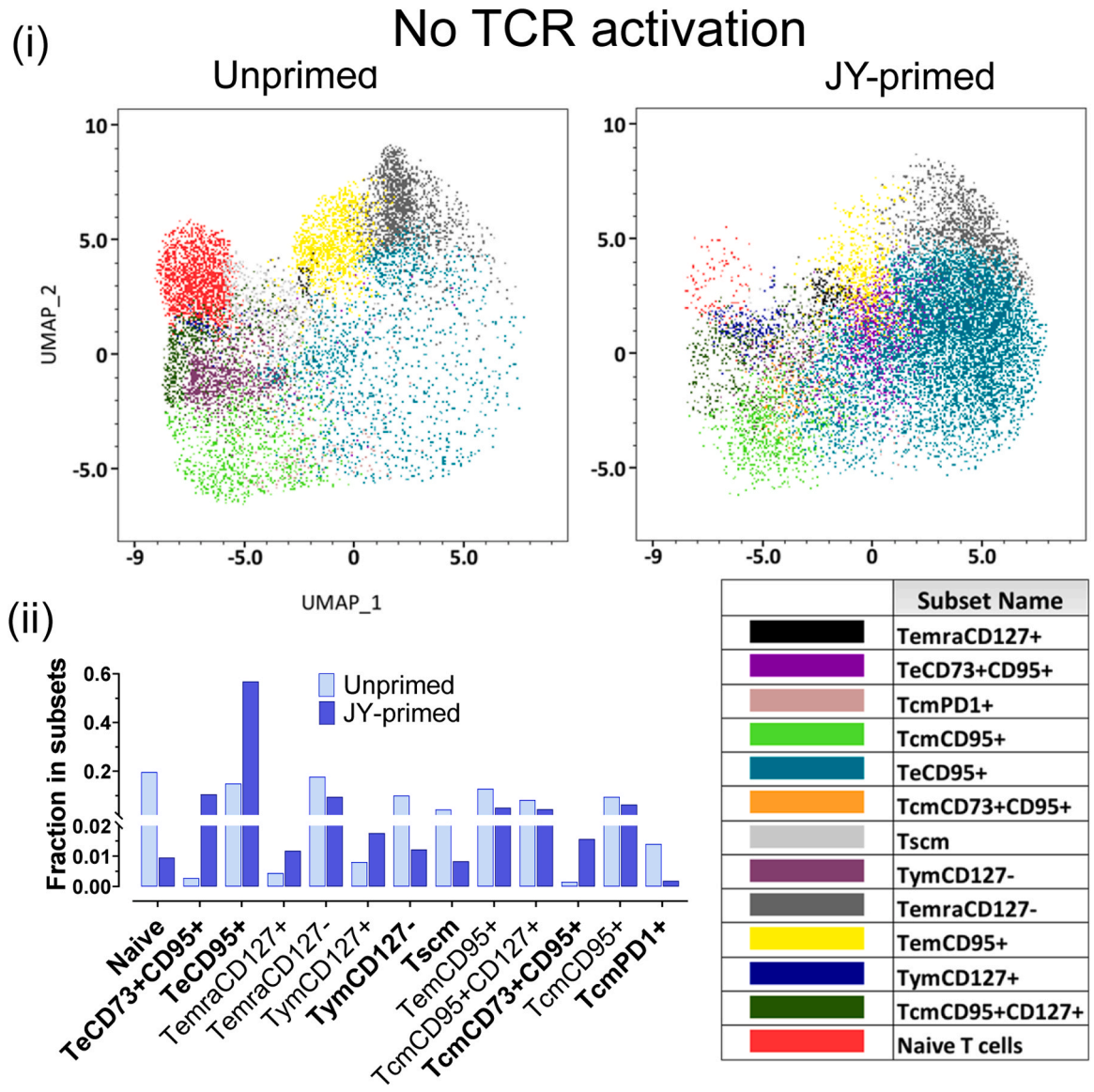

Fig. 4. Changes in CD8 + T cell subset sizes from human peripheral blood lymphocytes in response to allogeneic activation after one month (JY-primed). Cells were maintained with IL-2, and the allogeneic activation was repeated after two weeks. Samples are without acute CD3/CD28 activation. (i) The upper panel presents a UMAP cluster map with color-coded subpopulations, visually confirming maturation changes. (ii) The lower panel displays a bar chart showing changes in the same data set. All changes are statistically significant except those marked "ns" (non-significant). Subsets in bold indicate a large effect size, suggesting significant immunological effects. Non-bolded subsets represent medium or small effect sizes. There were no statistically negligible effect sizes.

upon activation of the CD3/CD28 TCR signal. Due to the nature of the *in vitro* system, which lacks the continuous naive T cell production from the thymus that occurs in vivo, there is a decrease in the naive T cell fraction, leading to their transformation into effector or memory cells. This is evidenced by a reduced fraction of naive T cells and an increased proportion of TeCD95 + and TeCD73 +CD95 + subsets. Although some cells may continue maturation from earlier stages initiated in the donor's body, the majority transform due to the *in vitro* TCR signal. Given that the donors were healthy and the CD3/CD28 antibody-coated bead signal robustly targets all TCR-expressing cells, the reliability of our research is confirmed.

We were particularly interested in monitoring changes within the memory subsets, especially the small intermediate memory subsets with higher Pgp levels. These changes occur as naive T cells transform into effector and memory cells and follow specific maturation pathways. Intermediate memory cells, such as TymCD127 + , Tscm, TemCD95 + , TcmCD95+CD127 + , and TcmPD1 + , decrease proportionally when there is insufficient supply from earlier cell stages. Conversely, subsets that increase are derived from earlier differentiation states, including short-lived effectors that later undergo apoptosis. This early maturation stage observed a significant increase in Pgp-carrying TcmCD95 + cells (from 9.5 % to 36.5 %). Additionally, the young memory TymCD127- subset, which also expresses high levels of CD95 and is closely related to the TcmCD95 + subset (Fig. 3i), showed a slight increase, making up nearly 10 % (from 9.9 % to 12.7 %) of the earliest Pgp-expressing memory subset in the PBL or TCR-activated PBL populations (Fig. 3ii). Supplementary figure 5 marks the direction of changes in the more significant Pgp-expressing subsets with a blue arrow.

3.4.2. Differentiation of long-lived CD8 + T cell subsets in JY-primed human peripheral blood lymphocyte cultures

The next stage of differentiation was assessed in one-month-old IL-2-expanded T cells, which were initiated through two cycles of JY-cell-primed mixed lymphocyte cultures. CD8 + T cell subsets in these cultures differentiated by recognizing JY-cell-presented allogeneic self-antigens, leading to a robust CD8 + T cell response. The one-month

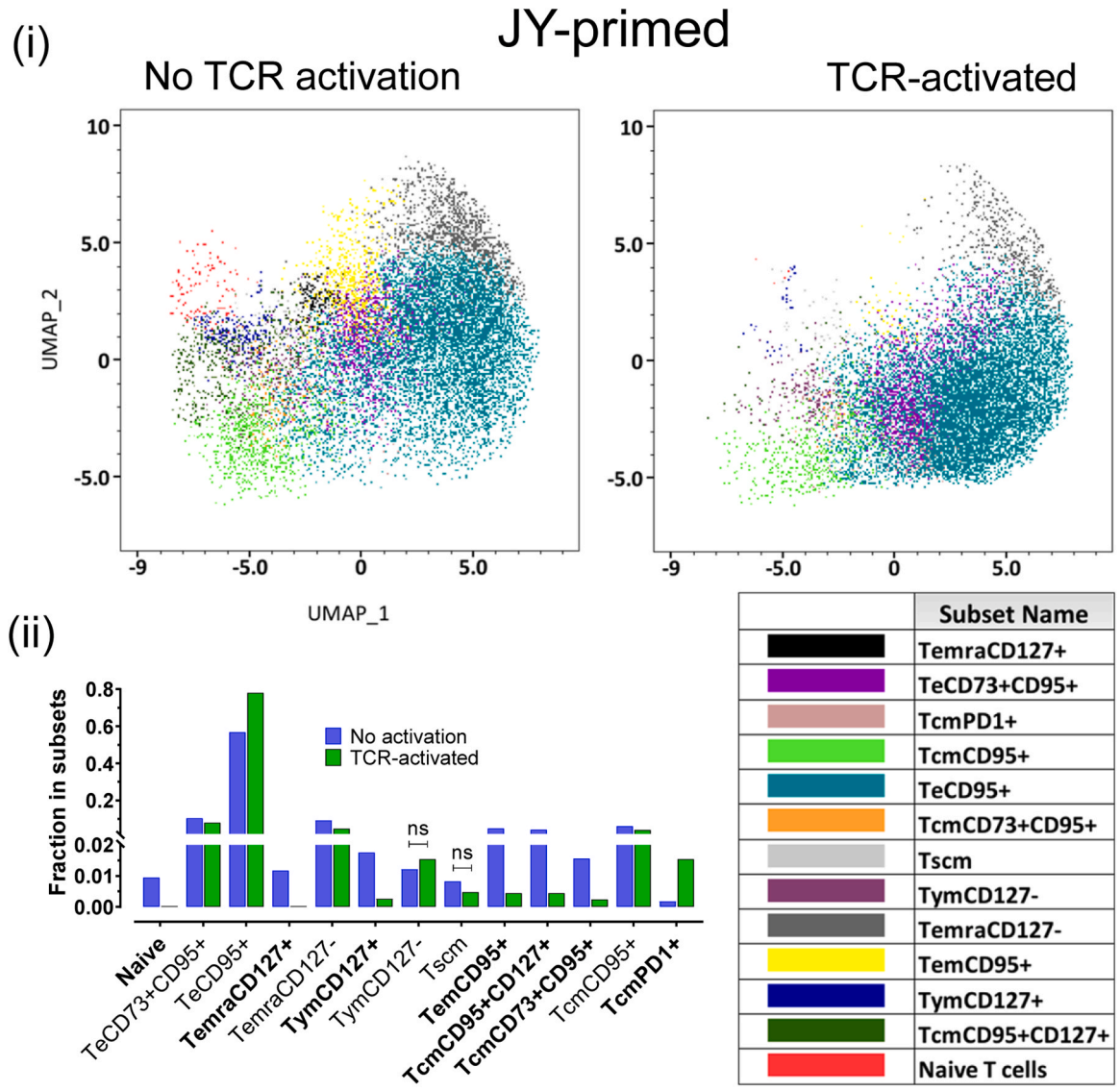

Fig. 5. Changes in CD8 + T cell subset sizes from JY-primed human lymphocytes in response to TCR activation after seventy-two hours. (i) The upper panel presents a UMAP cluster map with color-coded subpopulations, visually confirming maturation changes. (ii) The lower panel displays a bar chart showing changes in the same data set. All changes are statistically significant except those marked "ns" (non-significant). Subsets in bold indicate a large effect size, suggesting significant immunological effects. Non-bolded subsets represent medium or small effect sizes.

culture, supplemented with IL-2, promoted the differentiation and accumulation of long-lived memory subpopulations [28].

Fig. 4i shows a notable decrease in naive T cells and TymCD127-, TemCD95 + , TemraCD127 + , and TcmCD95+CD127 + subsets. In contrast, the most significant increases were observed in the TeCD95 + and TeCD73 +CD95 + subsets. Fig. 4ii reveals more subtle population changes, such as a reduction in the small subset of Pgp-expressing TcmPD1 + cells. Conversely, there was an increase in the TemraCD127 + subset and Pgp-expressing TymCD127 + and TcmCD73 +CD95 + subsets.

As a result of these changes, comparing JY-primed T cells after one month of maturation with unprimed PBLs showed a continued loss of naive T cells and a more pronounced increase in effector cells compared to the 72-hour acute TCR activation (see Fig. 3ii, Fig. 4ii, and Suppl. Fig. S5A-B). The previously increased TeCD95 + and TeCD73 +CD95 + subsets continued to expand, while the small TemraCD127 + subset grew significantly. Other memory subsets also changed, with long-lived memory cells emerging after the retraction phase. This led to increases in early TymCD127 + and TcmCD73 +CD95 + cells. Meanwhile, the broadly expanded TcmCD95 + central memory population decreased, along with the larger TymCD127- subset, which primarily expands into effector cells. The smaller TymCD127 + subset, which expresses high levels of Pgp, also transformed into TcmCD73 +CD95 + memory subsets.

3.4.3. Differentiation of late-stage CD8 + T cell subsets in TCR-reactivated, JY-primed cultures

To follow the latest maturation changes possible in this system, we activated the TCR signal by CD3/CD28 beads in the JY-primed one-month-old cultures.

In the upper Fig. 5i, the most prominent change is the repeated further increase in the TeCD95 + short-lived effector population, which, because of its short lifetime, must be produced from the intermediary smaller memory populations, especially since the naive precursors almost entirely disappear for this stage. This tendency, the decrease of the smaller intermediate populations, is also a noticeable alteration in the UMAP maps.

By comparing the TCR-activated and unactivated states in the JY-primed subset compositions in the lower Fig. 5ii, we can conclude that the recalled response of the T-cell memory population is remarkably

robust. This is evident as the peak response of TeCD95 + effector CTLs reaches nearly 80 %, compared to 40 % in the earlier unprimed conditions (Fig. 3ii). The established trend persists among the memory subsets during initial and recall TCR activation: long-lived small memory subsets express high levels of Pgp.

The most intriguing aspect of our research is the response of memory subsets to this late TCR activation. There is a notable loss of early maturation phase young memory TymCD127 + cells and their closely related central memory TcmCD73 +CD95 + cells, both of which had increased earlier. Remarkably, above the increasing CD95 + effectors, all other subpopulations decrease at this stage, except for the small Pgp-expressing TcmPD1 + subset. A significant and biologically meaningfully large size increase is observed in this late-stage central memory TcmPD1 + T cell subpopulation, the highest Pgp-expressing one. This subset remains small, comprising a few percent, similar to the earlier phase TymCD127 + and TcmCD73 +CD95 + small memory subsets, expressing all high levels of Pgp.

3.5. Ruxolitinib delays CD8 + T cell maturation

Ruxolitinib (RUX) is a kinase inhibitor commonly used in cancer and autoimmune therapies. It affects T-cell maturation by interfering with TCR Jak-1 and Jak-3 signaling. Our previous work (data not published) suggests RUX may interact with Pgp since we observed that it stimulates ATPase activity of the transporter. These findings prompted us to investigate the impact of RUX on CD8 + T cell maturation within the JY-priming system.

We conducted a series of experiments to evaluate the effects of RUX on CD8 + T cell maturation. Both unprimed and JY-primed cells were treated with RUX during TCR activation. We assessed the effects through multiple approaches.

First, we used UMAP maps to visualize the impact of RUX, which showed that RUX treatment preserved naive T cells during activation (Suppl. Fig. S6).

Next, ANOVA analysis results, displayed in violin plots for all subsets (Suppl. Fig. S7 and S8), indicated a pattern of maturation delay due to RUX. However, these changes were statistically insignificant.

Contingency table analysis supported the maturation-delaying effect of RUX (Suppl. Table S1), with significant differences observed in cell numbers. For example, the number of naive T cells in RUX-treated samples was consistently higher compared to those in pure TCR-activation samples, both in unprimed and JY-primed conditions.

We also quantified the observed effects in the contingency table by calculating the normalized cumulative change for RUX treatment during TCR activation across all subsets (Fig. 6). The cumulative difference for RUX treatment reflects the sum of differences observed at each of the four phases of the maturation process in the JY-priming TCR-activation experiments. Fig. 6 shows that subpopulations with positive cumulative differences increased over the four phases, while those with negative differences decreased compared to the untreated case. Significantly positive populations included naive T cells, TemraCD127 + , TemraCD127- cells, and Pgp-expressing TymCD127 + , Tscm, and TcmPD1 + cells (indicated in bold, with TeCD73 +CD95 + also positive but less significant). In contrast, the largest negatively affected population was the TeCD95 + effector cells, with a modest decrease in the TymCD127- subset. Thus, RUX treatment decreased the major short-lived effector subpopulation while preserving the small, long-lived Pgp-expressing memory populations, indicating that RUX delays CD8 + T cell maturation.

3.6. Changes in the naive population across the maturation phases

Fig. 7A shows that across the four major maturation stages, we have used, and during the maturation modifying ruxolitinib treatments, we could faithfully identify major subset changes characteristic of the adaptive CD8 immune response. For the acute TCR activation of the

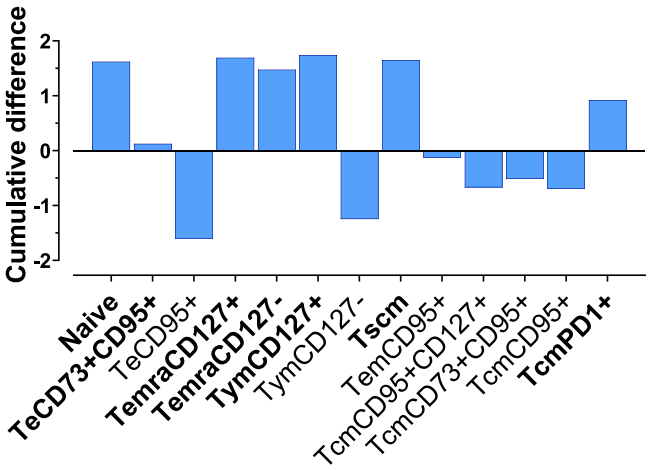

Fig. 6. Effect of Ruxolitinib. Subpopulations with positive values (in bold) increase their proportion to the end of the maturation process, and subpopulations with negative values decrease. To create this bar chart, the differences between RUX-treated and untreated values from the contingency table were first calculated. These differences were then summed across the four maturation phases: unprimed and unactivated, unprimed and TCR-activated, JY-primed and unactivated, JY-primed and TCR-activated. These summed differences were then normalized to the square root of the sum of squares. This normalization ensured that changes in the same direction were aggregated, resulting in larger values, while changes in opposite directions cancel each other.

PBLs, the initial population of the naive T cells decreased (from 19.7 % to 0.4 %; the numerical changes can be verified in Suppl. Fig. S5, while trends of the changes in Fig. 7). At one month, we measured 0.9 % naive, which became insignificant for the repeated "recall" TCR activation (0.03 %). Thus, at the end of the four maturation stages, the naive T cell population all transformed into more mature stage cells since there was no spare cell supply from the thymus. At every stage shown in Fig. 7A, RUX-treated samples exhibit an upward trend compared to their previous untreated stages, clearly indicating that RUX treatment delays naive T cell maturation.

During the one-month culture period, which involved two cycles of JY-cell allogeneic antigen presentation, a large number of allogeneic T-cell clones were generated due to the abundance of allogeneic antigens. This explains why the effector population continues to increase during the retraction phase rather than decrease, as would typically be expected during the contraction phase of a normal immune response. The fourth maturation phase, which generates a recall signal, involves reactivating all T cells using beads, similar to the activation process in the second phase of our maturation system. A limitation of this system is the continuous increase in effector cells, which contrasts with the expected contraction phase and may obscure some aspects of memory population behavior. However, the advantage lies in the robust and synchronous TCR activation induced by the abundance of allogeneic antigens, either through beads or JY cells, allowing for more reliable monitoring of the small memory populations.

3.7. Changes in the effector populations across the maturation phases

The two effector populations (TeCD95 +, TeCD73 +CD95 +) together increased significantly over the four maturation stages, rising from an initial 15.2–43.2 % following acute anti-CD3/CD28 bead-induced TCR activation (Fig. 7A and Suppl. Fig. S5). After one month of JY-cell allogeneic TCR activation, the effector populations expanded further to 67.4 %, and upon "recall" activation with anti-CD3/CD28 beads, they amplified even more to 86.1 %.

The predominant T effector population (TeCD95 +) in PBLs was initially 14.9 %, but following acute TCR activation, it increased to

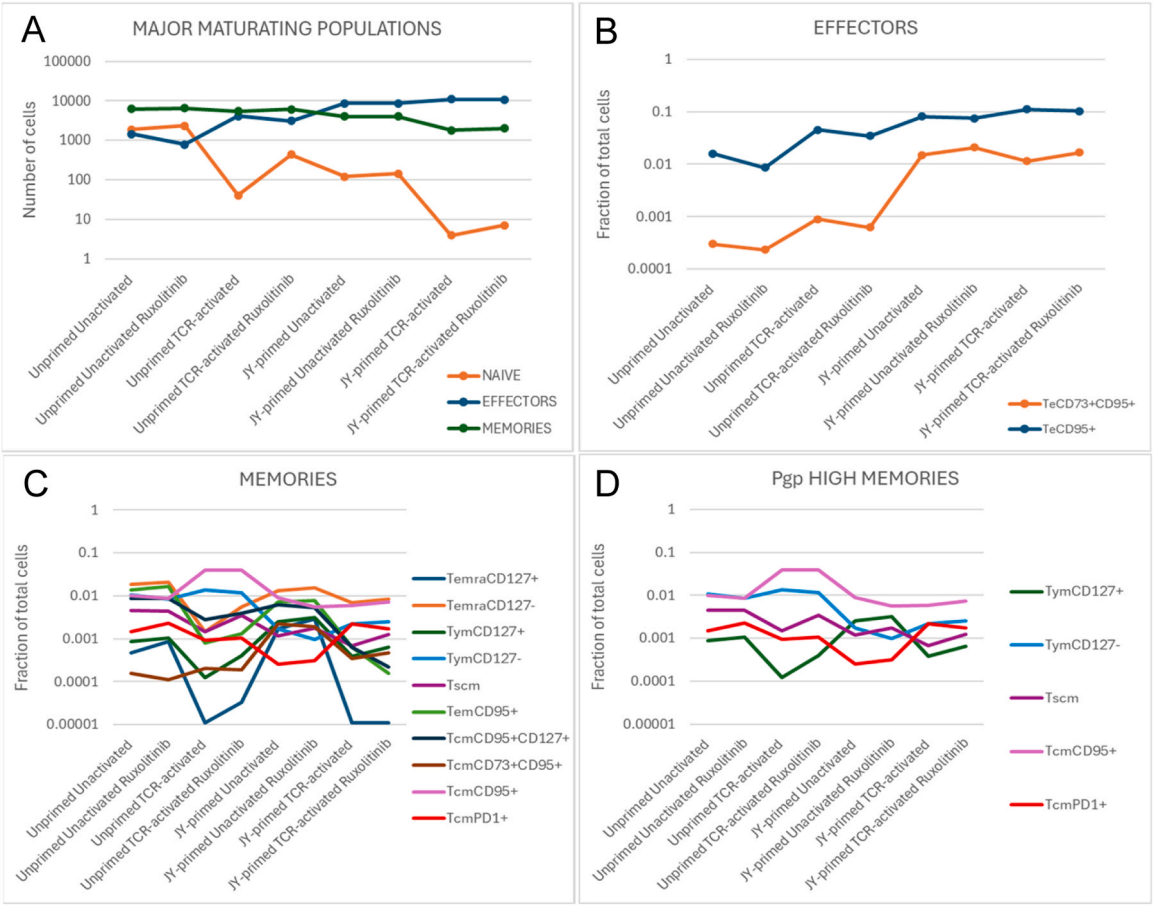

Fig. 7. Changes in CD8 + T cell subsets during in vitro differentiation and ruxolitinib treatment. The X-axis represents the maturation phases, while the Y-axis shows either the measured cell numbers (A) or the fractional size of the subsets within the total analyzed cells (B, C, D). The Y-axis is on a log scale to track changes in small memory subsets. (A) Cell numbers measured at different differentiation stages for the main CD8 + subsets. (B) Proportions of the two identified effector subtypes. (C) Proportions of the ten identified memory subtypes at different maturation stages. (D) The five highest Pgp-expressing memory subtypes identified among the memory subtypes shown in (C). Subset transformations occur during repeated TCR activations, eventually stabilizing their numbers.

42.4 %, and after one month, it further rose to 56.9 % (Fig. 7B and Suppl. Fig. S5). During the recall activation, this population further expanded, reaching 78 %. The other effector subset, TeCD73 +CD95 + , initially insignificant at 0.3 %, also grew into a reasonably notable population (8–11 %), though it remained only about a tenth the size of the dominant TeCD95 + subset.

RUX treatment consistently reduced overall effector cell generation, primarily due to its impact on the predominant TeCD95 + subset (Fig. 7A-B).

The effector populations appeared relatively homogeneous in their response to RUX treatment, consistently decreasing at each phase, in contrast to the naive T cells, which steadily increased. Most memory subsets also followed the trend of naive T cells, showing increases at different phases with RUX treatment. Interestingly, the smaller TeCD73 +CD95 + deviated from the typical effector response; while it decreased during the first two phases, it significantly expanded after one month and, like the naive T cells, increased in response to RUX treatment (Fig. 7B).

3.8. *Changes in the memory subsets across the maturation phases*

As PBLs progress through the maturation phases, the naive subset diminishes while effector populations expand significantly. Over the four maturation phases, the ten memory subsets collectively decrease from 65.2 % to 56.4 %, 31.7 %, and finally to 13.9 % (Fig. 7A and Suppl. Fig. S5). Initially, in PBLs, the six most prominent memory pools constituted 62.4 % of the total: TemraCD127- (17.7 %), TemCD95 + (12.8 %), TymCD127- (10 %), TcmCD95 + (9.5 %), TcmCD95+CD127 + (8.2 %), and the smaller Tscm subset (4.3 %). The remaining four memory subsets were each under 3 %: TcmPD1 + (1.4 %), TymCD127 + (0.8 %), TemraCD127 + (0.4 %), and TcmCD73 +CD95 + (0.1 %; Fig. 7C and D, and Suppl. Fig. S5).

Among the larger memory populations, TcmCD95 + showed the most significant early increase in the “expansion” phase, rising from 9.5 % to 36.5 %, while TymCD127- showed a modest increase from 10 % to 12.7 % during the acute signal phase at 72 hours (Fig. 7C and D, and Suppl. Fig. S5A). All other memory subsets decreased during this phase. However, these early increases in TcmCD95 + and TymCD127- were transient, with both subsets declining over one month. TcmCD95 + remained a significant subset through the maturation process, while TymCD127- eventually almost disappeared.

During the third, or “contraction,” phase, the ten memory subsets collectively shrank to 31.7 % (down from 65.1 % and 56.4 %; Fig. 7A, C, and D, and Suppl. Fig. S5B). The four major memory subpopulations that persisted were TemraCD127- (decreasing from 17.7 % to 9.4 %), TemCD95 + (dropping from 12.8 % to 5.0 %), TcmCD95+CD127 + (falling from 8.2 % to 4.3 %), and TcmCD95 + (declining from 9.5 % to 6.2 %), which together accounted for 24.9 % of the total cells. While these four subsets comprised 78.5 % of the total memory subsets, all experienced decreases during the retraction phase. Conversely, three smaller memory subsets increased: TymCD127 + (from 0.08 % to 1.8 %), TcmCD73 +CD95 + (from 0.01 % to 1.6 %), and TemraCD127 + (from 0.4 % to 1.2 %). Of these, Tym expressed high levels of Pgp while Tcm and Temra expressed low Pgp levels, similar to

naive T cells. The remaining three memory subsets, which all expressed high Pgp levels, decreased: TymCD127- (from 10 % to 1.2 %), Tscm (from 4.3 % to 0.08 %), and TcmPD1 + (from 1.4 % to 0.02 %).

In the final, fourth maturation phase, where cells are reactivated by CD3/CD28 beads, the highest Pgp-expressing memory subset, TcmPD1 + , increased again from 0.02 % to 1.5 %, alongside the other Pgp-high TymCD127- subset, which also rose to 1.5 % from 1.2 % (this latter is not significant; Fig. 7A, C and D, and Suppl. Fig. S5D). Meanwhile, the two largest memory subsets, TemraCD127- and TcmCD95 + , declined to 4.8 % and 4.1 %, respectively. Together, these four subsets accounted for 86.3 % of the total memory cells: out of these, TemraCD127- and TcmCD95 + made up 64.1 %, while TcmPD1 + and TymCD127- comprised 22.2 %. The remaining five memory subsets stabilized between 1.7 % and 3.4 %, except for TemraCD127 + , which nearly disappeared, representing just 0.06 % of the total memory population.

Figs. 7C and 7D illustrate that during successive maturation stages, both TcmCD95 + and TymCD127- populations increase following acute TCR activation, though this expansion is dampened by the kinase inhibitor RUX. This behavior is characteristic of a transit-amplifying expansion curve during acute TCR activation. Similar to tissue stem cells, which renew terminally differentiated tissue cells through asymmetric division, CD8 + T cells appear to follow a comparable behavior. In this context, TcmCD95 + and TymCD127- likely represent rapidly dividing transit amplifying cells, potentially derived from activated naive T cells (or possibly from Tscm cells, though this was not evident in our results).

Another growth pattern in Fig. 7 shows a decrease in certain cell populations following acute TCR activation, with RUX again mitigating this decline. These memory subsets include the nearly disappeared TemraCD127 + subset, the small TymCD127 + subset, the medium-sized TcmCD95+CD127 + subset, and the large TemCD95 + memory subset. All these subsets express high levels of CD127, suggesting their potential transformation into other subsets, such as effectors, in response to TCR signaling. Notably, from the literature it is postulated that CD127 downregulates TCR signaling [20], which may partially explain the observed growth patterns. These cells exhibit a similar pattern to naive T cells, which also express CD127.

A different trend shown in Fig. 7 is the increase in specific subsets after one month of culture, including TcmCD73 +CD95 + , TymCD127 + , TemraCD127 + , and TcmCD95+CD127 + . Interestingly, except for TcmCD73 +CD95 + , which remained stable under acute TCR signaling, the other subsets exhibited a decrease following acute TCR activation.

The final pattern in Fig. 7 pertains to the TcmPD1 + memory cells, a small but relatively stable subset that significantly expands following repeated long-term TCR signals.

These varied patterns suggest that while smaller memory subsets tend to increase, larger ones often decrease following repeated TCR signals.

4. Discussion

Pgp, a human cell-surface ABC transporter, is best known for its role in conferring multidrug resistance (MDR) in cancer cells, posing significant challenges to chemotherapy [3]. However, Pgp is also expressed in immune cells and plays critical roles in immune function [5]. Notably, a recent mouse study highlighted its importance in the development of immune memory [36]. Building on this knowledge, the present study investigates the expression of Pgp in human CD8 + memory T-cell subtypes at the single-cell protein level, aiming to deepen our understanding of its role in immune cell memory.

Human CTLs are primarily categorized into naive, effector, and memory cells based on their primary function and characteristics. Short-lived and quickly activated antigen-specific effector clones are generated by fast proliferation and eliminate antigen-carrying cells during the expansion phase of the immune response [37]. In the contraction phase, the short-lived effector cells dye and same-specificity memory cells appear to persistently provide the later recognition of the earlier observed antigen. These long-living memory cells are higher in number and more quickly transform into effectors than the same-specificity original long-living naive T cells [38–40].

We set up a model system to differentiate memory cells from peripheral blood and reconstitute the human adaptive CD8 + T-cell immune response *in vitro*. In long-term IL-2-supplemented mixed lymphocyte culture, we co-cultured growth-arrested antigen-presenting cells with peripheral lymphocytes. Our APCs were derived from the B-lymphoblastoid cell line JY expressing high levels of HLA-I A2 and co-receptors, thereby triggering a robust allogeneic cellular immune reaction. Flow cytometry analysis indicated that the JY-cell-mixed culture upregulated CD8 + , NK, and NK-T cells while downregulating B and CD4 + T cells. This MHC-I-restricted immune reaction notably increased Pgp expression on CD8 + , CD4 + , and B cells but decreased it on NK and NK-T cells, consistent with prior research [5,41,42].

We have observed the usual fractions of the known CD8 + T cell subsets in peripheral blood: 40 % naive, 20–25 % of both effector and Temra, and Tcm of the rest [43].

In our *in vitro* CTL maturation system, we generated four primary differentiation stages: 1) Unprimed and unactivated, 2) Unprimed and TCR-activated (CD3/CD28-bead triggered), 3) JY-primed (JY-cell-activated) and unactivated, and 4) JY-primed and TCR-activated. Additionally, we monitored the effects of ruxolitinib on each of these four stages. Stages 1 and 2 represent the acute phase of the adaptive immune response, while stage 3 models the memory phase, and stage 4 represents memory reactivation.

In this maturation system, we faithfully replicated the central dynamics observed during an adaptive immune response. A small number of long-lived naive and memory T cells transformed into a larger population of short-lived effector cells, which works to resolve potential infections and other life-threatening challenges. Simultaneously, maturing cells generate additional long-lived memory cells, which “remember” previous immune encounters, enabling a faster and more efficient response to future threats. This process led to a rapid decline in naive T cells, continuous production of effector cells, and the emergence of a heterogeneous memory cell population that gradually decreased in size overall. However, specific small subpopulations of long-lived cells demonstrated a relative increase within this shrinking memory population.

Naive T cells were depleted due to the lack of thymic-derived naive T cell replenishment *in vitro*. The population of short-lived effector cells expanded, primarily through continuous differentiation from naive T cells and, eventually, from various memory subpopulations. Within the heterogeneous memory population, specific small memory subpopulations expressing Pgp contributed to the longevity of the memory cell core.

By the conventional identification of the CD8 + peripheral blood lymphocytes, naive T cells are characterized by CD45RA+CD62L+ , central memory T cells by CD45RA-CD62L+ , effector T cells by CD45RA-CD62L-, and Temra cells by CD45RA+CD62L-. In this type of characterization, the naive and effector cells are reasonably well characterized, but memory cells are still heterogeneous, composed of many more minor subtypes. To distinguish small memory subsets, we utilized four more markers: CD73, CD95, CD127, and CD279. With this marker profile, we could identify the following 13 human CTL subsets: one naive, the two effectors TeCD95 + and TeCD73 +CD95 + , and ten memory cell populations TymCD127 + , TymCD127-, Tscm, TcmCD95 + , TcmCD73 +CD95 + , TcmCD95+CD127 + , TcmPD1 + , TemCD95 + , TemraCD127 + , and TemraCD127–.

Within these memory populations, in the acute phase, the central memory TcmCD95 + subset generated the most, with a smaller amount of the young TymCD127- subset, probably preceding the previous one. In the memory phase, the small population of the young memory

TymCD127 + generated the most. The TcmPD1 + central memory cell population, which carries the late marker, expanded significantly during the later stages of the TCR-reactivated memory-recall phase. The stem cell memory Tscm pool maintained a considerable 2–4 % stable subpopulation along the maturation phases within the dynamically transforming heterogeneous memory populations.

We used CD73 as a marker to identify young memory cells, known for their Pgp expression, as described by Murata [13]. Tym cells were initially identified by high ALDH1 expression, a recognized stemness marker [44]. They were further characterized by elevated CD73, ALDH1, and Pgp expression, all associated with stem cell-like properties. CD73, an ecto-nucleotidase, generates immunosuppressive adenosine from ATP released by damaged cells and acts as a co-signaling molecule in T cells. It is linked to long-lived memory T cells that differentiate into tissue-resident cells [45,46] and modulates T-cell activation. Tym populations exhibit high proliferative capacity, self-renewal, ALDH1 activity, and drug resistance [13]. Notably, TCR activation reduces CD127 expression in chemo-resistant CTL subsets, distinguishing activated TymCD127 − cells from non-activated TymCD127 + cells [20].

To identify the Tscm (stem cell memory) population, we used the CD95 marker, mainly known for its apoptosis induction role in T cells; however, it also can promote cell survival [47]. Tscm cells, initially identified in graft-versus-host disease [15], are commonly recognized by markers such as CD45RA, CD62L, CD127, and CD95, exhibiting properties of self-renewal, multipotency, and proliferative potential [7,18, 48]. The Tscm and Tym cells are closely related, but the latter is considered an earlier-state memory cell [13]. Both express CD95, Pgp, and other common markers; consequently, slight contamination of the Tym cells in the Tscm or other Tcm populations can bias memory populations into considering them as long-lived memory subclasses. It was demonstrated previously that Tym and Tscm cells differentiate into central memory and effector memory T cells, not only effector cells, making the memory population diverse [13,18].

We used CD127 to identify IL-7 receptor-expressing cells, which transmit survival signals and are crucial for the homeostatic proliferation of naive and memory T cells [20,49]. CD127 is also a marker for memory and effector T cells, with its downregulation observed during activation or exposure to IL-15 [20,50]. Therefore, identifying CTL subsets highlights the presence of distinct maturing CTL subtypes, which could be leveraged for immunotherapy applications.

To identify late-stage maturation T cells, we used PD-1 (CD279), a marker overexpressed in exhausted CTLs during chronic infections and cancer [37]. PD-1 dampens TCR signaling to prevent autoimmunity during prolonged activation and repeated TCR stimulation, marking the later maturation stage of exhausted T cells (Tex) [51]. Although Tex cells are often considered unresponsive, checkpoint therapies and the discovery of stem-like Tex cells (Tex-stem) highlight their potential functionality. These self-renewing, proliferative, PD-1-expressing Tex--stem cells underpin long-term responses within the terminal Tex subset [52].

The TcmPD1 + cells we characterized likely belong to these exhausted stem cells (Tex-stem). In other studies, similar cells have been categorized as exhausted precursors (Tex-pre) due to their continued expression of CD62L [51]. In our experiments, the TcmPD1 + cells exhibited similar characteristics, including the highest levels of Pgp expression. We believe this can be explained by these cells' acquired or preserved stemness, which allows them to divide asymmetrically. Exhausted T cell precursors also share general surface markers and transcriptional profiles with long-lived cells. Tym, Tscm, and Tcm cells, which exhibit long-lived characteristics, express markers similar to Tex precursors, such as CD27, CD28, and CXCR3 [13,37].

The role of the multidrug-resistant protein Pgp in CTL subsets remains an active area of investigation. This study shows that Pgp is most highly expressed in the TcmPD1 + , Tscm, TymCD127-, and TymCD127 + CTL subsets. The presence of Pgp on these cells suggests it plays a crucial role in their chemo-immune efflux capacity, protection against reactive oxygen species, and maintenance of quiescence while retaining robust proliferative potential. Together, these functions may contribute to the stemness properties of stem-like memory cells [5,7,20, 36]. Collectively, these findings highlight the importance of Pgp in the maturation and persistence of CTL subsets.

The repetitive TCR, co-stimulatory, and interleukin receptor signals via the JAK/STAT signaling pathways impact CTL maturation. We applied the JAK1/JAK2-specific kinase inhibitor ruxolitinib to explore its effect on memory cell differentiation and to provide insights into its pharmaco-immunological applications. Crosstalk of these receptor signaling biases JAK/STAT routes toward effector or memory cell differentiation. MF diseases and GVHD are both characterized by overactivated JAK/STAT signaling and the early exhaustion of adaptive immune surveillance. Applying RUX in these diseases, which releases the signaling load from the JAK/1/JAK2 pathways, provided less effector activation [53,54]. We also gained results indicating that preventing JAK1/JAK2 activation decreases effector cell production and a shift of differentiation toward the memory cell population. It is known that effector cell production is enhanced by IL-12, which signals via JAK1 and JAK2 [55–57]. IL-7 and IL-15 provide memory cell proliferation and maintenance. These interleukines signal via JAK1 and JAK3 routes [58,59]. Consequently, inhibiting JAK1/JAK2 may shift differentiation from effector cells toward memory cells, an observation strongly supported by our data. Remarkably, in an anti-tumor model, applying IL-7 and IL-12 together in a tumor-targeted manner could enhance the anti-tumor effect while avoiding frequently experienced interleukin side effects [57]. Testing the more JAK2-specific inhibitors fedratinib and pacritinib in our *in vitro* CTL maturation system would be interesting.

In Fig. 7, RUX delayed T-cell differentiation by increasing naive cell numbers while reducing effector cells. Memory subsets exhibited distinct patterns: smaller subsets behaved more like naive cells, expanding with activation, whereas larger subsets resembled effector cells, contracting with repeated TCR stimulation. These findings suggest a small, quiescent core memory pool that matures heterogeneously in response to repeated TCR signals, maintaining long-term stability through asymmetric division and cytokine modulation.

For example, in the case of a COVID-19 "cytokine storm," RUX has been shown to improve outcomes in patients with a high COVID-19 Inflammation Score (CIS), identifying hyperinflammatory patients who may benefit from treatment [17]. This suggests that RUX inhibits effector CTL maturation, which is consistent with our findings. Importantly, we observed that while effector differentiation decreased, the maturation of the small core memory subset increased in the presence of RUX during TCR activation, indicating that preserving the functional memory pool may contribute to CTL persistence in later inflammatory responses.

In another example, PD-1-expressing cells decreased in the presence of RUX during the contraction phase in JY-primed CD3/CD28-bead reactivated samples but not earlier, reflecting PD-1's role as a late activation marker. This is consistent with previous studies suggesting that RUX reduces the fraction of PD-1-expressing T cells, which has been observed in settings like graft-versus-host disease and graft-versus-leukemia, where late-stage effectors are predominant [14]. Besides the previous literature data, which are supported by our results, RUX also exhibits broader immunomodulatory effects. It includes PD-L1 downregulation in the tumor microenvironment and inhibition of macrophage M2 polarization [53]. All of these are beneficial in cancer therapy but can be controversial in the context of autoimmune therapy.

Our findings indicate that subsets such as TemraCD127-, TemraCD127 + , and TemCD95 + were significantly downregulated during TCR activation. However, exposure to RUX tended to increase the percentage of TemraCD127 + cells. Similar trends were observed for the TymCD127 + , TemraCD127-, and TemCD95 + subsets (Suppl. Fig. S7). These results are in agreement with prior research showing that CD127 expression is downregulated following activation or exposure to IL-15

[20]. RUX's ability to delay effector maturation and increase CD127-expressing populations may also explain its synergistic effect with venetoclax, a Bcl-2 inhibitor, in recent studies linking increased IL-7R alpha/CD127 expression to improved acute lymphoblastic leukemia therapy outcomes [60].

Our most significant observations are as follows: 1) Upon TCR reactivation without chemotherapy, small Pgp-expressing memory subpopulations are continuously and dynamically generated. Over time, these long-lived, maturing cells are preserved within the heterogeneous CD8 + memory subclasses. 2) The earliest of these long-lived small memory subsets among CD8 + T cells are the TymCD127 + cells. 3) The PD1 + late population also represents a significant Pgp-expressing small memory subset, alongside the earlier TymCD127 + subpopulation, while the TymCD127-, Tscm, and TcmCD95 + cells are potentially more committed to rapid proliferation as daughter cells.

Based on our observations, we hypothesize that these Pgp-expressing small populations form the core of self-renewing, asymmetrically and slowly dividing quiescent memory subpopulations. Similar stemness-property holding quiescent cells were observed in studies of Boddupalli et al. [61]. Upon receiving TCR signals, these potentially quiescent cells, through asymmetric division, generate rapidly dividing committed transit-amplifying cells, which eventually mature into short-lived effector cells. However, with repeated TCR signaling, these memory subsets evolve into more aged, long-lived populations expressing later maturation markers, such as PD-1.

We propose that long-lived core memory T cells are best preserved in low-redox environments, such as the bone marrow, supporting long-term memory even decades after infection [6,7,61]. These cells can also persist in other low-redox tissues, like the skin or gut, as tissue-resident memory cells (Trm) [61]. This functional adaptation unifies concepts of immune memory and aligns with Soerens's observation that PD-1, despite marking exhaustion, does not restrict cell division, allowing memory T cells to surpass the Hayflick limit and maintain robust, adaptive immunity, with a promise for effective anti-cancer vaccination [62].

In conclusion, the TCR activation process reveals distinct maturation patterns among various CD8 + T cell subsets with known lifespans. Early TCR activation transforms long-lived naive T cells into effector and central memory cells, with a notable increase in the short-lived TeCD95 + , and TeCD73 +CD95 + , and the long-lived Pgp-high TcmCD95 + subsets. The one-month maturation phase further differentiates and transforms these cells, increasing Temra and advanced memory subsets while highlighting the high Pgp expression in specific small but long-lived memory subsets in the earlier TymCD127 + and the later TcmPD1 + cells. The pronounced recall response in JY-primed cells underscores the robust adaptive capabilities of memory T cells compared to their initial activation.

This study highlights the intricate relationship between repeated TCR activation and CTL maturation dynamics. Measuring Pgp expression in the presence of ruxolitinib may have significant therapeutic implications, especially for optimizing immune responses, improving chemotherapy efficacy, and optimizing preventive vaccinations.

Funding

Financial support to Z.B. was provided by the University of Debrecen (OTKA Bridging Research Fund 2022; Science Financing Support 2022–23; Publication Science Support Program 2023–24; DETKA Scientific Research Bridging Fund 2024). A Stipendium Hungaricum scholarship (2020–24) supported the work of K.B. and P.S.

CRediT authorship contribution statement

Sándor Baráth: Writing – review & editing, Resources, Methodology. **Parvind Singh:** Writing – review & editing, Visualization, Software, Methodology, Formal analysis. **Kipchumba Biwott:** Writing – review & editing, Writing – original draft, Visualization, Validation, Software, Methodology, Investigation, Formal analysis, Data curation. **Zsolt Bacso:** Writing – review & editing, Writing – original draft, Visualization, Validation, Supervision, Software, Resources, Project administration, Methodology, Funding acquisition, Formal analysis, Conceptualization. **Zsuzsanna Hevessy:** Writing – review & editing, Resources, Methodology. **James Nyabuga Nyariki:** Writing – review & editing.

Declaration of Competing Interest

The authors declare that they have no known competing financial interests or personal relationships that could have appeared to influence the work reported in this paper.

Acknowledgment

We extend our sincere thanks to Marianna Száraz-Széles from the Department of Laboratory Medicine, Rita Katalin Utasi-Szabó and Edina Nagy from the Department of Biophysics and Cell Biology, and Anett Mázló from the Department of Immunology, all of them from the University of Debrecen, Hungary, whose dedication and contributions were instrumental in the completion of this article.

Appendix A. Supporting information

Supplementary data associated with this article can be found in the online version at doi:10.1016/j.biopha.2024.117780.

Data Availability

Data will be made available on request.

References

[1] B. Sarkadi, L. Homolya, G. Szakacs, A. Varadi, Human multidrug resistance ABCB and ABCG transporters: participation in a chemoimmunity defense system, Physiol. Rev. 86 (4) (2006) 1179–1236.
[2] M. Iqbal, H.L. Ho, S. Petropoulos, V.G. Moisiadis, W. Gibb, S.G. Matthews, Pro-inflammatory cytokine regulation of P-glycoprotein in the developing blood-brain barrier, PLoS One 7 (8) (2012) e43022.
[3] M.M. Gottesman, T. Fojo, S.E. Bates, Multidrug resistance in cancer: role of ATP-dependent transporters, Nat. Rev. Cancer 2 (1) (2002) 48–58.
[4] E. Bello-Reuss, S. Ernest, O.B. Holland, M.R. Hellmich, Role of multidrug resistance P-glycoprotein in the secretion of aldosterone by human adrenal NCI-H295 cells, Am. J. Physiol. Cell Physiol. 278 (6) (2000) C1256–1265.
[5] M. Bossennec, A. Di Roio, C. Caux, C. Menetrier-Caux, MDR1 in immunity: friend or foe? Oncoimmunology 7 (12) (2018) e1499388.
[6] C. Thurm, B. Schraven, S. Kahlfuss, ABC Transporters in T Cell-Mediated Physiological and Pathological Immune Responses, Int J. Mol. Sci. 22 (17) (2021).
[7] C.J. Turtle, H.M. Swanson, N. Fujii, E.H. Estey, S.R. Riddell, A distinct subset of self-renewing human memory CD8+ T cells survives cytotoxic chemotherapy, Immunity 31 (5) (2009) 834–844.
[8] A. Alsuliman, M. Muftuoglu, A. Khoder, Y.O. Ahn, R. Basar, M.R. Verneris, P. Muranski, A.J. Barrett, E. Liu, L. Li, K. Stringaris, D. Armstrong-James, H. Shaim, K. Kondo, N. Imahashi, B. Andersson, D. Marin, R.E. Champlin, E.J. Shpall, K. Rezvani, A subset of virus-specific CD161(+) T cells selectively express the multidrug transporter MDR1 and are resistant to chemotherapy in AML, Blood 129 (6) (2017) 740–758.
[9] K. Devine, E. Villalobos, C.J. Kyle, R. Andrew, R.M. Reynolds, R.H. Stimson, M. Nixon, B.R. Walker, The ATP-binding cassette proteins ABCB1 and ABCC1 as modulators of glucocorticoid action, Nat. Rev. Endocrinol. 19 (2) (2023) 112–124.
[10] G. Kooij, J. Kroon, D. Paul, A. Reijerkerk, D. Geerts, S.M. van der Pol, B. van Het Hof, J.A. Drexhage, S.J. van Vliet, L.H. Hekking, J.D. van Buul, J.S. Pachter, H. E. de Vries, P-glycoprotein regulates trafficking of CD8(+) T cells to the brain parenchyma, Acta Neuropathol. 127 (5) (2014) 699–711.
[11] A. Ramos, S. Sadeghi, H. Tabatabaeian, Battling Chemoresistance in Cancer: Root Causes and Strategies to Uproot Them, Int J. Mol. Sci. 22 (17) (2021).
[12] L.K. Mackay, A.T. Stock, J.Z. Ma, C.M. Jones, S.J. Kent, S.N. Mueller, W.R. Heath, F.R. Carbone, T. Gebhardt, Long-lived epithelial immunity by tissue-resident memory T (TRM) cells in the absence of persisting local antigen presentation, Proc. Natl. Acad. Sci. USA 109 (18) (2012) 7037–7042.
[13] K. Murata, T. Tsukahara, M. Emori, Y. Shibayama, E. Mizushima, H. Matsumiya, K. Yamashita, M. Kaya, Y. Hirohashi, T. Kanaseki, T. Kubo, T. Himi, S. Ichimiya, T. Yamashita, N. Sato, T. Torigoe, Identification of a novel human memory T-cell

population with the characteristics of stem-like chemo-resistance, Oncoimmunology 5 (6) (2016) e1165376.
[14] I. Veletic, S. Prijic, T. Manshouri, G.M. Nogueras-Gonzalez, S. Verstovsek, Z. Estrov, Altered T-cell subset repertoire affects treatment outcome of patients with myelofibrosis, Haematologica 106 (9) (2021) 2384–2396.
[15] Y. Zhang, G. Joe, E. Hexner, J. Zhu, S.G. Emerson, Host-reactive CD8+ memory stem cells in graft-versus-host disease, Nat. Med 11 (12) (2005) 1299–1305.
[16] F. La Rosee, H.C. Bremer, I. Gehrke, A. Kehr, A. Hochhaus, S. Birndt, M. Fellhauer, M. Henkes, B. Kumle, S.G. Russo, P. La Rosee, The Janus kinase 1/2 inhibitor ruxolitinib in COVID-19 with severe systemic hyperinflammation, Leukemia 34 (7) (2020) 1805–1815.
[17] J. Hammersen, S. Birndt, K. Dohner, P. Reuken, A. Stallmach, P. Sauerbrey, F. La Rosee, M. Pfirrmann, C. Fabisch, M. Weiss, K. Trager, H. Bremer, S. Russo, G. Illerhaus, D. Dromann, S. Schneider, P. La Rosee, A. Hochhaus, The JAK1/2 inhibitor ruxolitinib in patients with COVID-19 triggered hyperinflammation: the RuxCoFlam trial, Leukemia 37 (9) (2023) 1879–1886.
[18] L. Gattinoni, E. Lugli, Y. Ji, Z. Pos, C.M. Paulos, M.F. Quigley, J.R. Almeida, E. Gostick, Z. Yu, C. Carpenito, E. Wang, D.C. Douek, D.A. Price, C.H. June, F. M. Marincola, M. Roederer, N.P. Restifo, A human memory T cell subset with stem cell-like properties, Nat. Med 17 (10) (2011) 1290–1297.
[19] M. Dusseaux, E. Martin, N. Serriari, I. Peguillet, V. Premel, D. Louis, M. Milder, L. Le Bourhis, C. Soudais, E. Treiner, O. Lantz, Human MAIT cells are xenobiotic-resistant, tissue-targeted, CD161hi IL-17-secreting T cells, Blood 117 (4) (2011) 1250–1259.
[20] R.F. Kudernatsch, A. Letsch, M. Guerreiro, M. Lobel, S. Bauer, H.D. Volk, C. Scheibenbogen, Human bone marrow contains a subset of quiescent early memory CD8(+) T cells characterized by high CD127 expression and efflux capacity, Eur. J. Immunol. 44 (12) (2014) 3532–3542.
[21] Z. Bacso, L. Bene, A. Bodnar, J. Matko, S. Damjanovich, A photobleaching energy transfer analysis of CD8/MHC-I and LFA-1/ICAM-1 interactions in CTL-target cell conjugates, Immunol. Lett. 54 (2-3) (1996) 151–156.
[22] H. Spits, J.E. de Vries, C. Terhorst, A permanent human cytotoxic T-cell line with high killing capacity against a lymphoblastoid B-cell line shows preference for HLA A, B target antigens and lacks spontaneous cytotoxic activity, Cell Immunol. 59 (2) (1981) 435–447.
[23] Y. Dong, T.N. Denny, HLA-A2-restricted human CD8(+) cytotoxic T lymphocyte responses to a novel epitope in vaccinia virus that is conserved among orthopox viruses, J. Infect. Dis. 194 (2) (2006) 168–175.
[24] W.S. Khalaf, M. Garg, Y.S. Mohamed, C.M. Stover, M.J. Browning, In vitro Generation of Cytotoxic T Cells With Potential for Adoptive Tumor Immunotherapy of Multiple Myeloma, Front Immunol. 10 (2019) 1792.
[25] H. Lu, B. Tang, Y. He, W. Zhou, J. Qiu, Y. Li, Identification of HLA-A* 1101-restricted cytotoxic T lymphocyte epitopes derived from epidermal growth factor pathway substrate number 8, Mol. Med Rep. 14 (6) (2016) 4999–5006.
[26] A. Lustig, T. Manor, G. Shi, J. Li, Y.T. Wang, Y. An, Y.T. Liu, N.P. Weng, Lipid Microbubble-Conjugated Anti-CD3 and Anti-CD28 Antibodies (Microbubble-Based Human T Cell Activator) Offer Superior Long-Term Expansion of Human Naive T Cells In Vitro, Immunohorizons 4 (8) (2020) 475–484.
[27] G. Gellen, E. Klement, K. Biwott, G. Schlosser, G. Kallo, E. Csosz, K. F. Medzihradszky, Z. Bacso, Cross-Linking Mass Spectrometry on P-Glycoprotein, Int J. Mol. Sci. 24 (13) (2023).
[28] V. Kalia, S. Sarkar, Regulation of Effector and Memory CD8 T Cell Differentiation by IL-2-A Balancing Act, Front Immunol. 9 (2018) 2987.
[29] A. Emmaneel, K. Quintelier, D. Sichien, P. Rybakowska, C. Maranon, M.E. Alarcon-Riquelme, G. Van Isterdael, S. Van Gassen, Y. Saeys, PeacoQC: Peak-based selection of high quality cytometry data, Cytom. A 101 (4) (2022) 325–338.
[30] E. Becht, L. McInnes, J. Healy, C.A. Dutertre, I.W.H. Kwok, L.G. Ng, F. Ginhoux, E. W. Newell, Dimensionality reduction for visualizing single-cell data using UMAP, Nat. Biotechnol. (2018).
[31] S. Van Gassen, B. Callebaut, M.J. Van Helden, B.N. Lambrecht, P. Demeester, T. Dhaene, Y. Saeys, FlowSOM: Using self-organizing maps for visualization and interpretation of cytometry data, Cytom. A 87 (7) (2015) 636–645.
[32] N. Cieri, G. Oliveira, R. Greco, M. Forcato, C. Taccioli, B. Cianciotti, V. Valtolina, M. Noviello, L. Vago, A. Bondanza, F. Lunghi, S. Marktel, L. Bellio, C. Bordignon, S. Bicciato, J. Peccatori, F. Ciceri, C. Bonini, Generation of human memory stem T cells after haploidentical T-replete hematopoietic stem cell transplantation, Blood 125 (18) (2015) 2865–2874.
[33] L. Gattinoni, D.E. Speiser, M. Lichterfeld, C. Bonini, T memory stem cells in health and disease, Nat. Med 23 (1) (2017) 18–27.
[34] E. Lugli, L. Gattinoni, A. Roberto, D. Mavilio, D.A. Price, N.P. Restifo, M. Roederer, Identification, isolation and in vitro expansion of human and nonhuman primate T stem cell memory cells, Nat. Protoc. 8 (1) (2013) 33–42.
[35] Y. Xia, A. Liu, W. Li, Y. Liu, G. Zhang, S. Ye, Z. Zhao, J. Shi, Y. Jia, X. Liu, Y. Guo, H. Chen, J. Yu, Reference range of naive T and T memory lymphocyte subsets in peripheral blood of healthy adult, Clin. Exp. Immunol. 207 (2) (2022) 208–217.
[36] M.L. Chen, A. Sun, W. Cao, A. Eliason, K.M. Mendez, A.J. Getzler, S. Tsuda, H. Diao, C. Mukori, N.E. Bruno, S.Y. Kim, M.E. Pipkin, S.B. Koralov, M.S. Sundrud, Physiological expression and function of the MDR1 transporter in cytotoxic T lymphocytes, J. Exp. Med 217 (5) (2020).
[37] E. Lugli, G. Galletti, S.K. Boi, B.A. Youngblood, Stem, Effector, and Hybrid States of Memory CD8(+) T Cells, Trends Immunol. 41 (1) (2020) 17–28.
[38] S.C. Jameson, D. Masopust, Understanding Subset Diversity in T Cell Memory, Immunity 48 (2) (2018) 214–226.
[39] D. Masopust, L.J. Picker, Hidden memories: frontline memory T cells and early pathogen interception, J. Immunol. 188 (12) (2012) 5811–5817.
[40] N.P. Restifo, L. Gattinoni, Lineage relationship of effector and memory T cells, Curr. Opin. Immunol. 25 (5) (2013) 556–563.
[41] S.S. Pendse, D.M. Briscoe, M.H. Frank, P-glycoprotein and alloimmune T-cell activation, Clin. Appl. Immunol. Rev. 4 (1) (2003) 3–14.
[42] J.C. Zhang, F. Xie, X.H. Yu, Z.Y. Deng, Y. Wang, P. Liang, L. Sun, F.X. Zhang, Expression levels of P-glycoprotein in peripheral blood CD8+ T lymphocytes from HIV-1-infected patients on antiretroviral therapy, Int J. Mol. Med 33 (2) (2014) 431–440.
[43] J.L. Reading, F. Galvez-Cancino, C. Swanton, A. Lladser, K.S. Peggs, S.A. Quezada, The function and dysfunction of memory CD8(+) T cells in tumor immunity, Immunol. Rev. 283 (1) (2018) 194–212.
[44] M.A. Gomez-Salazar, Y. Wang, N. Thottappillil, R.W. Hardy, M. Alexandre, F. Holler, N. Martin, Z.N. Gonzalez-Galofre, D. Stefancova, D. Medici, A.W. James, B. Peault, Aldehyde Dehydrogenase, a Marker of Normal and Malignant Stem Cells, Typifies Mesenchymal Progenitors in Perivascular Niches, Stem Cells Transl. Med 12 (7) (2023) 474–484.
[45] F. Fang, W. Cao, W. Zhu, N. Lam, L. Li, S. Gaddam, Y. Wang, C. Kim, S. Lambert, H. Zhang, B. Hu, D.L. Farber, C.M. Weyand, J.J. Goronzy, The cell-surface 5′-nucleotidase CD73 defines a functional T memory cell subset that declines with age, Cell Rep. 37 (6) (2021) 109981.
[46] E. Schneider, R. Winzer, A. Rissiek, I. Ricklefs, C. Meyer-Schwesinger, F.L. Ricklefs, A. Bauche, J. Behrends, R. Reimer, S. Brenna, H. Wasielewski, M. Lauten, B. Rissiek, B. Puig, F. Cortesi, T. Magnus, R. Fliegert, C.E. Muller, N. Gagliani, E. Tolosa, CD73-mediated adenosine production by CD8 T cell-derived extracellular vesicles constitutes an intrinsic mechanism of immune suppression, Nat. Commun. 12 (1) (2021) 5911.
[47] V. Risso, E. Lafont, M. Le Gallo, Therapeutic approaches targeting CD95L/CD95 signaling in cancer and autoimmune diseases, Cell Death Dis. 13 (3) (2022) 248.
[48] L. Xu, Y. Zhang, G. Luo, Y. Li, The roles of stem cell memory T cells in hematological malignancies, J. Hematol. Oncol. 8 (2015) 113.
[49] K.M. Huster, V. Busch, M. Schiemann, K. Linkemann, K.M. Kerksiek, H. Wagner, D. H. Busch, Selective expression of IL-7 receptor on memory T cells identifies early CD40L-dependent generation of distinct CD8+ memory T cell subsets, Proc. Natl. Acad. Sci. USA 101 (15) (2004) 5610–5615.
[50] F. Parween, S.P. Singh, H.H. Zhang, N. Kathuria, F.A. Otaizo-Carrasquero, A. Shamsaddini, P.J. Gardina, S. Ganesan, J. Kabat, H.A. Lorenzi, T.G. Myers, J. M. Farber, Chemokine positioning determines mutually exclusive roles for their receptors in extravasation of pathogenic human T cells, bioRxiv (2023).
[51] E. Terrabuio, E. Zenaro, G. Constantin, The role of the CD8+ T cell compartment in ageing and neurodegenerative disorders, Front Immunol. 14 (2023) 1233870.
[52] F. Gounari, K. Khazaie, TCF-1: a maverick in T cell development and function, Nat. Immunol. 23 (5) (2022) 671–678.
[53] H. Chen, M. Li, N. Ng, E. Yu, S. Bujarski, Z. Yin, M. Wen, T. Hekmati, D. Field, J. Wang, I. Nassir, J. Yu, J. Huang, D. Daniely, C.S. Wang, N. Xu, T.M. Spektor, J. R. Berenson, Ruxolitinib reverses checkpoint inhibition by reducing programmed cell death ligand-1 (PD-L1) expression and increases anti-tumour effects of T cells in multiple myeloma, Br. J. Haematol. 192 (3) (2021) 568–576.
[54] T. Teshima, D. Hashimoto, Separation of GVL from GVHD -location, location, location, Front Immunol. 14 (2023) 1296663.
[55] J.M. Curtsinger, D.C. Lins, M.F. Mescher, Signal 3 determines tolerance versus full activation of naive CD8 T cells: dissociating proliferation and development of effector function, J. Exp. Med 197 (9) (2003) 1141–1151.
[56] J.M. Curtsinger, C.S. Schmidt, A. Mondino, D.C. Lins, R.M. Kedl, M.K. Jenkins, M. F. Mescher, Inflammatory cytokines provide a third signal for activation of naive CD4+ and CD8+ T cells, J. Immunol. 162 (6) (1999) 3256–3262.
[57] S. Kang, A. Mansurov, T. Kurtanich, H.R. Chun, A.J. Slezak, L.R. Volpatti, K. Chang, T. Wang, A.T. Alpar, K.C. Refvik, O.I. Hansen, G.J. Borjas, H.N. Shim, K. T. Hultgren, S. Gomes, A. Solanki, J. Ishihara, M.A. Swartz, J.A. Hubbell, Engineered IL-7 synergizes with IL-12 immunotherapy to prevent T cell exhaustion and promote memory without exacerbating toxicity, Sci. Adv. 9 (48) (2023) eadh9879.
[58] L. Belarif, C. Mary, L. Jacquemont, H.L. Mai, R. Danger, J. Hervouet, D. Minault, V. Thepenier, V. Nerriere-Daguin, E. Nguyen, S. Pengam, E. Largy, A. Delobel, B. Martinet, S. Le Bas-Bernardet, S. Brouard, J.P. Soulillou, N. Degauque, G. Blancho, B. Vanhove, N. Poirier, IL-7 receptor blockade blunts antigen-specific memory T cell responses and chronic inflammation in primates, Nat. Commun. 9 (1) (2018) 4483.
[59] T.A. Waldmann, S. Dubois, M.D. Miljkovic, K.C. Conlon, IL-15 in the Combination Immunotherapy of Cancer, Front Immunol. 11 (2020) 868.
[60] L. Courtois, A. Cabannes-Hamy, R. Kim, M. Delecourt, A. Pinton, G. Charbonnier, M. Feroul, C. Smith, G. Tueur, C. Pivert, E. Balducci, M. Simonin, L.H. Angel, S. Spicuglia, N. Boissel, G.P. Andrieu, V. Asnafi, P. Rousselot, L. Lhermitte, IL-7 receptor expression is frequent in T-cell acute lymphoblastic leukemia and predicts sensitivity to JAK inhibition, Blood 142 (2) (2023) 158–171.
[61] C.S. Boddupalli, S. Nair, S.M. Gray, H.N. Nowyhed, R. Verma, J.A. Gibson, C. Abraham, D. Narayan, J. Vasquez, C.C. Hedrick, R.A. Flavell, K.M. Dhodapkar, S. M. Kaech, M.V. Dhodapkar, ABC transporters and NR4A1 identify a quiescent subset of tissue-resident memory T cells, J. Clin. Invest 126 (10) (2016) 3905–3916.
[62] A.G. Soerens, M. Kunzli, C.F. Quarnstrom, M.C. Scott, L. Swanson, J.J. Locquiao, H. E. Ghoneim, D. Zehn, B. Youngblood, V. Vezys, D. Masopust, Functional T cells are capable of supernumerary cell division and longevity, Nature 614 (7949) (2023) 762–766.